Research article

A coating machine for coating filaments with bioactive nanomaterials for extrusion 3D printing

Ulf Tilman Strähle [a,b,*], Norbert Pütz [a], Matthias Hannig [a]

[a] Clinic of Operative Dentistry, Periodontology and Preventive Dentistry, Saarland University Hospital, 66421, Homburg, Saarland, Germany
[b] Synoptic Dentistry, Saarland University Hospital, 66421, Homburg, Saarland, Germany

A B S T R A C T

Extrusion printing based on biocompatible filaments offers a wide variety of targeted medical and dental applications in the area of personalized medicine, if combined with bioactive nanomaterials. However, this requires filament to be coated with bioactive nanomaterial. This study introduces a concept of a machine to coat filament with bioactive nanomaterials and its application. A machine was constructed with modules manufactured using additive manufacturing. A filament spool of polylactide (PLA) or glycol-modified polyethylene terephthalate (PETG) was transported through a copper tube, with the outer surface of the filament heated to the appropriate glass transition temperature to incorporate added nanomaterials such as nano-hydroxyapatite (nHA) or nano-fluorapatite(nFA). Coatings with nHA led to an increase in diameter of around 3 μm, while coatings with nFA increased the diameter by 4 μm. Printing of cubes with a standard extrusion printer platform using PLA or PETG filaments with added nHA or nFA has been successfully carried out. Scanning electron microscope (SEM) images of coated filaments and printed cubes showed an irregular distribution of nHA or nFA, which could be verified by energy dispersive X-ray analysis (EDX). Adding and adjusting bioactive nanomaterials to filament with a coating machine for filament proved to generate printable filaments. With the wide range of possible applications by different nanomaterials it is anticipated that extrusion printing can cover needs for personalized medicine and dentistry.

1. Introduction

3D printing processes are also suitable for the production of pharmaceuticals [1]. When manufacturing printed tablets using 3D printing processes, it is possible to precisely deliver a single or several active pharmaceutical ingredients (API) by individually designing separate layers [2]. In addition, 3D printing processes also enable the implementation of personalized medicine [2]. At present, the field of activity and objectives of the personalized medicine are defined differently: On the one hand, fields of activity can be identified in which comprehensive analyses are used to optimize the administration and dosage of medication for individual patients [3]. On the other hand, personalized medicine is understood as genomic and phenotypic medicine with a focus on manipulating signaling cascades and understanding cell behavior [4]. Different printing methods of drugs offer the possibility of adapting dosage and application forms to individual patient needs [2] and can thus meet both definitions of personalized medicine [3,4]. Changes in dosage and release of an active substance can be made depending on a patient's metabolization rate and adverse drug reactions can be reduced by coordinating the composition of active substances with other pharmaceuticals [2]. In addition binder jetting [5], drugs can also be produced experimentally using stereolithography printing processes [6]. The disadvantages of this method are residual uncured methacrylate- or acrylate-based monomers that remain after printing [7] as well as the need for openings in the printed object to allow liquid resin to escape [8,6], which can cause allergies [6]. The material extrusion process (MEX), which is extended by hot melt

* Corresponding author. Clinic of Operative Dentistry, Periodontology and Preventive Dentistry, Saarland University Hospital, 66421, Homburg, Saarland, Germany.
  E-mail addresses: ulf.straehle@uks.eu, ulf.straehle@icloud.com (U.T. Strähle).

extrusion (HME) and in which biocompatible thermoplastics can be used, is another suitable 3D printing process for pharmaceutical production [1]. The production of thermoplastic polymers for MEX printing processes is carried out using the HME process, which makes it possible to combine both processes [9]. The advantages of this process lie in the use of polymers approved by the Food and Drug Administration (FDA), such as PLA [1].

For 3D printing in dentistry, it seems desirable to use the MEX 3D printing process and to combine health-safe, biocompatible carrier materials [1] with bioactive, dental nanomaterials such as nano-hydroxyapatite (nHA) or nano-fluorapatite (nFA) [10,11,12]. Nano-hydroxyapatite particles are already used in toothpastes for tooth whitening and for the treatment of hypersensitive teeth [11] by covering open dentinal tubules through the formation of a mineralized protective layer [13]. They are also able to reduce tooth sensitivity after bleaching [14]. In addition, nHA has remineralization effects, especially in initial enamel lesions [15] and in vitro in the outer parts of white spot lesions [16]. However, this remineralization potential of HA and fluoride is also viewed controversially and its equivalence is questioned [17]. Rather, HA is suitable as a bone replacement material: an osteogenic effect of HA was first demonstrated in 1920 by F. H. Albee et al. [18]. Synthetic HA is a complete analog of HA found in bone, which explains its osteo-cunductive potential and biocompatibility [19]. Accordingly, it is suitable as a filling material for the regeneration of bone defects [11], but has a slow degradation rate [19]. Nano-hydroxyapatite also promotes attachment of the periodontal ligament, which enables periodontal or implantological suitability [20]. A layer of nHA on the surface of dental implants reduces inflammatory reactions due to modulating properties of HA [21]. If a dental implant is coated with HA, this has an increasing effect on osseointegration and osteoinduction, resulting in a longer implant life compared to an uncoated implant [11]. This is caused by dipole-dipole interactions of HA with water, proteins and collagen, which cause surface adsorption of these substances [22].

By replacing the hydroxyl group with fluoride ions, HA with a molecular formula of $Ca_{10}(PO_4)_6(OH)_2$ [23] is converted into fluorapatite (FA) with a molecular formula of $Ca_{10}(PO_4)_6F_2$ [24,23,11]. Both compounds belong to calcium apatites and have bioactive properties without toxic or allergic potential [11]. FA is characterized by increased chemical and physical stability compared to HA [25]. It was already successfully used in 1947 by J. F. McClendon et al. to reduce the formation of new carious lesions [26]. In an in vitro study, rod-shaped nano-fluorapatite particles were antibacterially effective against Fusobacterium nucleatum and Streptococcus mutans with high cytocompatibility [27]. If fluorapatite is used as an active ingredient in a protective varnish, this leads to an increase in fluoride concentration and micro hardness [28].

For 3D printing in dentistry HA could be used as a scaffold material and for periodontal regeneration [20]. FA on the other hand is suitable for remineralization and prevention of carious lesions [26].

As nHA or nFA cannot be used directly for MEX 3D printing printing a carrier material such as PLA or PETG is needed. By this, bioactive printing material with dental suitability could be harvested [29]. PLA is approved by the FDA for medical use [1]. It was already used in vivo in 1970 for the treatment of jaw fractures in dogs and blow-out fractures in monkeys [30] and in 1971 as a suture material in medicine [31]. In the human body, PLA is degraded by hydrolysis of the polymer chains, and this slow process contributes to PLA's three to five year shelf life in vivo [32]. PLA has high mechanical strength and porosity [19]. An increase in the bioactive surface area of PLA can be achieved by adding inorganic particles [33]. Hereby, the osteoinductive property of PLA can be improved by adding HA [19]. Due to its extracellular degradation, PLA is also suitable as a drug carrier and can be used in dentistry as a scaffold material for bone regeneration or as a coating for improved osseointegration of dental implants [32].

PETG offers an alternative to PLA, as it has good processing and biocompatible properties in addition to higher temperature resistance [34]. PETG is biodegradable and ductile [35]. This can be seen in tensile tests with a higher degree of plasticity and stress values compared to PLA [36]. Polyethyleneterephthalate (PET) is already used in medicine as a degradable vascular replacement, but is unsuitable for extrusion printing due to its crystallinity [37]. Modification with glycol creates PETG with the same biocompatibility compared with PET [37], an amorphous, non-crystalline polymer [35]. In dentistry, PETG is used in the thermoforming process to produce dental splints [35]. PLA seems to be a suitable as a carrier material for a bioactive filament due to its wide range of medical applications as a bone substitute material [32,38,39] and PETG as a possible material for splints [35] or crowns due to its higher temperature resistance [34].

As mentioned above a suitable printing process for drug production is extrusion printing, which is enhanced by HME, which existed in pharmacy since the 1970s [40]. In this process, polymers with active pharmaceutical ingredients (APIs) are mixed and pressed through an extruder [5]. There are two basic types of extruders: a RAM type or a screw type [9]. In the RAM type, heated material is pressed through a cylinder with a small opening by means of a piston [9]. In terms of screw type extruders, an extruder can be a single screw extruder (SSE) with one screw, a twin screw extruder (TSE) with two screws or a multi screw extruder (MSE) with several screws [40]. After material of choice is added via a funnel [9], it is mixed with a polymer by the feed screw in a cylinder and undergoes a feed movement according to the principle of an Archimedean screw, which causes the mixture to be extruded through a nozzle [40]. What both extrusion processes have in common is that the extruded product strand is further processed in the conventional pharmaceutical industry in the form of pellets or thin films [40], or that the extracted product strand is processed into a filament spool for extrusion desktop printing [41]. Since thermoplastic polymers for extrusion printing are produced using the HME process, a combination with a desktop extrusion printer is possible [9]. For this purpose, polymers with APIs are mixed and pressed through an extruder, resulting in a strand of both materials [5]. In addition to the production of pharmaceuticals, printing processes coupled with HME also enable the possibility of producing drug-eluting implants [9]. Weisman et al. produced filament using HME processes that releases antibiotics and chemotherapeutic drugs against osteomyelitis [42]. Mathew et al. took a similar approach by printing a catheter made of filament obtained using the HME process with added tetracycline hydrochloride to protect against bacterial infections [43]. It is also possible to produce biomimetic scaffolds [19], which serve as placeholders made of biocompatible materials that can be degraded to restore own tissue [44]. W. Wang et al. used a mixture of PLA and nano-hydroxyapatite to produce composite scaffolds using extrusion printing processes, which showed potential for repairing femoral defects in vivo [45]. The new bone formation achieved by these scaffolds was

superior to scaffolds made of pure PLA [46].

Extrusion printing processes coupled with HME has also been investigated in dental research [47,48]. Berger et al. produced printed caps made of polycaprolactone, polyvinyl alcohol, and sodium fluoride for fluoride release in an in vitro study, which were adapted to the crown shape of extracted human teeth and enabled tooth remineralization [47]. In a first clinical study on volunteers, Liang et al. produced individualized mouthguards by using extrusion printing, in which saliva eluted active ingredients [48]. However, these mouthgards, which were produced using an extrusion printer with a nozzle diameter of 0.35 mm, proved to be too inaccurate [48]. A more precise adjustment can be achieved by changing to a nozzle with a diameter of 0.25 mm [49]. In extrusion printing the smaller the nozzle diameter, the less favorably the printing result is influenced by irregularities in the filament diameter. This is due to the fact that an average filament diameter is used to calculate the G-code and deviations lead to excesses or deficiencies in the printing result and weight [41].

For this reason, the previously described methods of admixture using HME processes are not appropriate for precision printing in medicine and dentistry, as there are fluctuations in the filament diameter, with deviations of 1.65 mm $\pm$ 0.10 mm in Liang et al. [48], 1.75 $\pm$ 0.05 mm in Wang et al. [46,45], 1.75 mm $\pm$ 0.10 mm in Weisman et al. [42] or 1.75 mm $\pm$ 0.15 mm in the study by Berger et al. [47].

Another approach to enrich filament with nanoparticles was pursued by Vidakis et al. [50,51] and Petousis et al. [52,53]. Silver nanoparticles were successfully added to PLA to achieve an antimicrobial effect [51]. For filament production, the components were mixed, dried in a vacuum oven and processed into filament using an SSE, which was then dried [51]. The diameter of the filament produced was 1.74 mm with a standard deviation of $\pm$0.04 mm [51]. However, the entire manufacturing process took more than 52 h [51]. For the addition of tungsten carbide to PLA to improve mechanical properties, Vidakis et al. mixed these components, which were then dried, processed into filament using an SSE and then crushed into pellets [50]. These pellets were again processed into filament in a second extrusion process, which resulted in a uniform distribution of tungsten carbide. However, this process also requires more than 24 h [50]. A similarly time-consuming manufacturing process was also shown in the work of Petousis et al. in the production of multifunctional nanocomposite from copper oxide and cellulose nanofibers [53]. For the production of filament from PETG with antimony-doped tin oxide, the time required for the manufacturing process was reduced to around 8 h [52]. However, the diameter of the filament obtained was between 1.65 mm and 1.85 mm [52]. Further processes such as filament impregnation require subsequent, time-consuming drying [54,55], or are only intended for coating with aluminum and copper [56], which is why they are also excluded.

To date, no method has been published that describes the production of small amounts of individual mixtures of bioactive materials for medical or dental purposes and, thus enables the implementation of personalized medicine [3,4] by adapting the dosage of bioactive nanomaterials to the individual needs of patients [2]. For this reason, it appears necessary to develop a new process that enables the coating of small quantities like PLA and PETG with nHA or nFA to produce filament-based, biomimetic and bioactive 3D printing materials. At the same time, this process should also enable the implementation of personalized medicine [3,4], in that the dosage of nanomaterials can be adapted to the respective, individual needs of patients [2]. In addition, quantities of just a few grams are sufficient for the production of dental splints or individual crowns from patient-specific dental filament. Rapid prototyping (RP) can be used as a cost-effective solution [57] to produce a machine suitable for coating filament. In this process, computer aided design (CAD) of a prototype is saved in.STL format, which enables later implementation using 3D printing processes [58]. This is also known as rapid prototyping manufacturing (RPM) [59]. The goal of this investigation is the design of a functional prototype of this machine, a so-called alpha prototype [60], which is referred to as coating machine for filament in this work.

The concept of interest (COI), a trend-setting concept in the manufacturing process [61], includes the following points for this work.

(i) There should only be slight changes in filament diameter after coating.
(ii) It should be possible to customize the product to the needs of patients and to produce small quantities of filament should be possible.
(iii) The coating of filament should be carried out with a coating machine for filament.
(iv) The print quality of coated filaments should be comparable to that of uncoated filaments with coated filaments showing a high degree of purity.
(v) The coating of the filament should take less than 1 h so that a chairside use in dental practice is possible.

The successful feasibility of the newly developed manufacturing process with the coating machine developed for this purpose was subsequently demonstrated with the proof of concept (PoC) [61].Therefore, filament passed through a heated copper tube, whereby added nanoparticles adhered to the surface of the filament and coated filament was created. This could be verified by SEM images and EDX analysis.

2. Materials and methods

2.1. Selection of basic components to produce bioactive filaments

Nanomaterials such as hydroxylapatite or fluorapatite are suitable for medical and dental purposes [10,11,12]. Hydroxylapatite can be used as a scaffold material for periodontal regeneration [20] or as bone replacement material [18,11,19]. In the present study, hydroxylapatite was used as a nanopowder from Kalichem (Kalident Powder 100 1ST B (17 kGy), Italy). S&C Polymer GmbH kindly provided 10 g nano-fluorapatite powder (Charge: RC2206379; S&C Polymer GmbH, Germany). Fluorapatite is suitable for

remineralization and avoiding carious lesions [26] due to antibacterial properties [27].

Thermoplastic polymers such as PETG and PLA are suitable as carrier materials for an addition of the nanomaterials mentioned above. ColorFabb_HT clear (Colorfabb B.V., Netherlands) was chosen as the PETG filament, since this material has an approval of the FDA [62], with a permanent temperature of 100 °C [63] and, thus is suitable for possible temperature loads of up to 90 °C in the oral cavity [64]. This PETG filament (Table 1) is a transparent filament, which facilitate examination of effects of adding mixtures, without the possible influence of added dyes. A future use for the production of temporary dental crowns is conceivable, whereby nFA is released during abrasion and attrition and remineralization potential is created [65,26,11,27,66]. Usages as bioactive splint material is also conceivable, since PETG is already used as a material for retainers in orthodontics [35].

In medicine, PLA is used as a suture material [38]. It is also suitable as a scaffold material for bone regeneration [32,38,39], whereby osteo-inductive properties can be increased by adding inorganic particles, as nHA [18,21,33]. In this study, extrudr PLA NX2 white (Extrudr FD3D GmbH, Lauterach, Austria) was used. Despite its white color this filament is certified by the FDA [67]. A colored PLA filament (Table 1) has been selected to examine any effects of additions to colored filament. A later use of PLA for crown production is not possible due to the low glass transition temperature of a maximum of 60 °C [39].

Both filaments showed a diameter of 1.75 mm, so that the later used printer (Original Prusa i3 MK3S+, Prusa Research a.s., Czech Republic) can process them in the extrusion printing process. For the selected filaments, corresponding print settings are already stored in the software required for printing (Prusaslicer version 2.5.0, Prusa Research a.s., Czech Republic).

Table 1
Mechanical properties of used filament.

filament	colorFabb_HT clear, 1.75 mm (colorFabb B.V., Netherlands)	extrudr PLA NX2 white (Extrudr FD3D GmbH, Austria)	Prusament PETG signal white, Prusament PETG Clear (Prusa Research a.s., Czech Republic)
usage for	coating machine for filament - sieve insert -pestle -mounting for copper tube as carrier material/filament for coating machine	coating machine for filament -sieve insert -pestle as carrier material/filament for coating machine	all other components for the coating machine for filament except -sieve insert -pestle -mounting for copper tube
FDA approval	FDA food contact compliance [62]	FDA compliant [67]	none
density (ISO 1183)	1.2 g/cm^3 [63]	1.3 g/cm^3 [67]	1.27 g/cm^3 [68]
elongation at break (Tensile, ASTM D638)	210 % [63]		
elongation at break (Tensile, ISO 527-1A)	26 % [63]		
elongation at strength (ISO 527)		4 % [67]	
elongation at yield point (ISO 527-1)			horizontal: 5.1 ± 0.1 %, vertical: 5.1 ± 0.1 % [68],
flexural modulus (E-Modulus, ISO 178)	N/A [63]	2650 MPa [67]	horizontal: 1700 ± 100 MPa, vertical: 1600 ± 100 MPa [68],
flexural modulus (Tensile, ASTM D790)	1,575 MPa [63]		
flexural strength (Charpy Notch, ISO 179)	6.4 kJ/m^2 [63]		horizontal: 66 ± 2 MPa, vertical: 70 ± 1 MPa [68],
flexural strength (ISO 178)			
Izod impact strength (Izod Notch, ASTM D256)	860 J/m [63]		
nominal elongation at break (ISO 527-2)		19 % [67]	horizontal: 6 ± 1 kJ/m^2, vertical: 3 ± 1 kJ/m^2 [68],
notched impact strength (ISO 179/1eA)		7 kJ/m^2 [67]	
stress at break (ISO 527)		23 MPa [67]	
tensile modulus (E-Modulus, ISO 527)		2600 MPa [67]	
tensile strength (E-Modulus, ISO 527)	50 MPa [63]	47 MPa [67]	46 ± 1 MPa [68]
tensile strength (Tensile, ASTM D638)	43 MPa [63]		horizontal: 47 ± 2 MPa, vertical: 50 ± 1 MPa [68],
tensile yield strength (E-Modulus, ISO 527)			
unnotched impact strength (ISO 179/1eU)		no break [67]	
Youngs Modulus (Tensile, ASTM D638)	N/A [63]		
Youngs Modulus (Tensile, ISO 527-1A)	1500 MPa [63]		

Due to different test standards on the part of the manufacturers, only a limited comparison of the mechanical properties of the filaments is possible.

2.2. Selection of process technologies for coating filaments

In order to coat filament, various process techniques had to be combined: On the one hand, mechanical process techniques were used, including the propulsion of the filament, pulverizing of nanomaterials through vibration and uniting of filament and nanomaterials.

On the other hand, a thermal process technology was used to merge filament and nanomaterials. Since deviations of filament's diameter should be as small as possible to increase the printing quality [41], only the surface of the filament was heated. Therefore, glass transition temperatures of PETG or PLA were chosen to enable adhesion of nanomaterials, without melting them, yet. This should allow particles of nHA or nFA to be incorporated into the surface-heated filament layer.

2.3. Development of a coating machine for filament

A coating machine was designed accordingly by segmented designs [69]. Modules were assigned tasks of the process techniques previously set up (Fig. 1). Each modules were designed with a skeletonized construction in mind. This design enables material-saving work. The individual modules were manufactured using RPM [59] with the aim of assembling them into a functional alpha prototype [60]. Each module was drawn with a 3D software (SketchUp, Trimble®, U.S.A) and a G-Code was created with PrusaSlicer 2.5.0 (Prusa Research a.s., Prag, Tschechische Republik). The standard settings of the slicing software were retained without minimizing the printing time. Minimizing printing time can lead to the application of additional layers, which can have an unfavorable effect on mechanical loads [70]. To fill internal structures, PrusaSlicer version 2.5.0 allows a selection of different infills. Here, primarily gyroid and partially cubic patterns were chosen, as these have good mechanical properties [71]. The larger the module created, the lower the density of the infill was selected in order to reduce the printing time. The G-Code was used to print individual modules with a 3D printer (Original Prusa i3 MK3S, Prusa Research a.s., Czech Republic) and an E3D V6 brass nozzle with a diameter of 0.4 mm on a double-sided textured PEI powder-coated spring steel sheet (Original Prusa i3 MK3/S/+ and MK2.5/S heatbeds, Prusa Research a.s., Czech Republic). Since layer thicknesses and overlaps of printed structures within an object have a significant influence on stiffness [72], the printing process was visually monitored. The prints were produced at a room temperature of 18–22 °C. Each module was checked for functionality after successful completion and assembly. Additive manufacturing of individual modules was carried out to
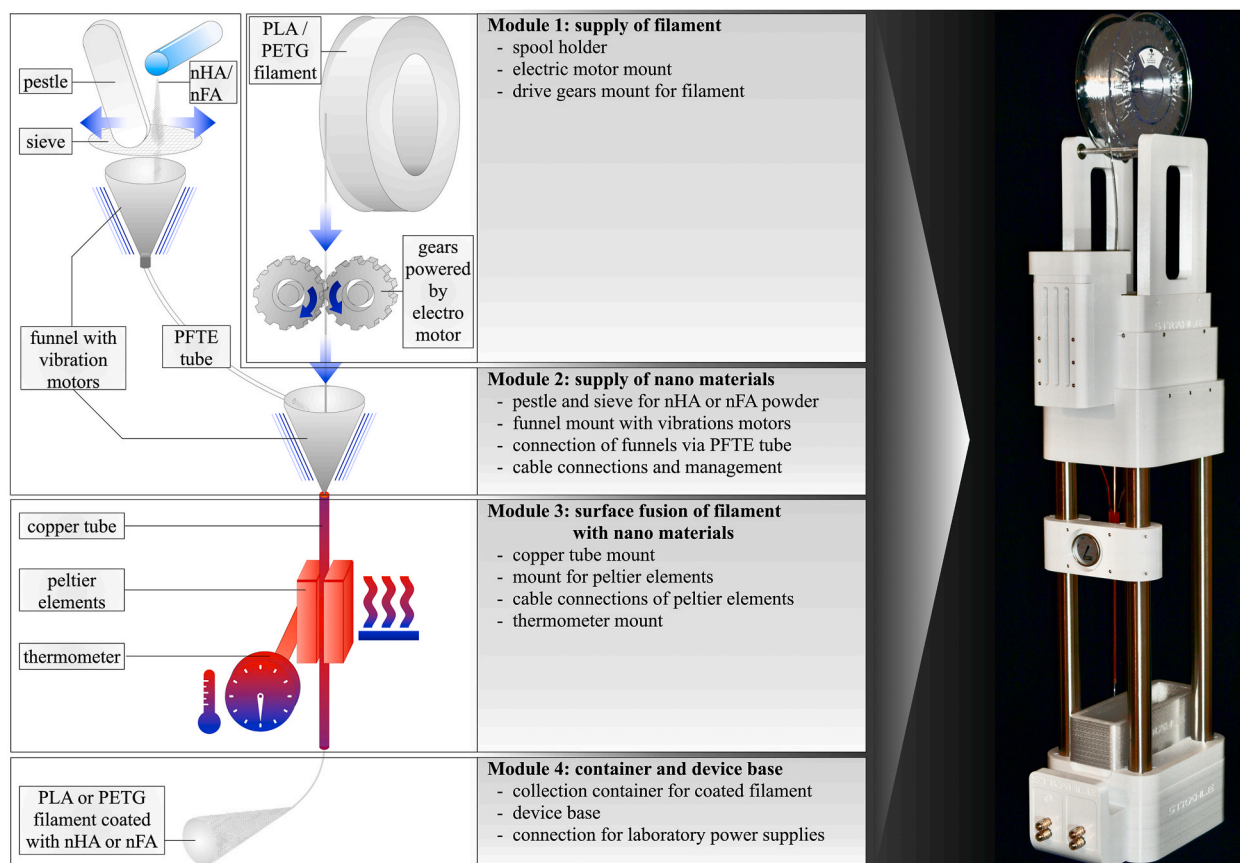

Fig. 1. Implementation of various process techniques in modules for a coating machine for filament.

assemble a functional alpha prototype [60], and then testing its function on coating PETG and PLA filaments with nHA and nFA.

Prusament PETG signal white (Prusa Research a.s., Prague, Czech Republic) was chosen as the base material for the modules (Table 1), as its heating bed temperature of 80 °C ± 10 °C [68] correlates with thermal stress resistance. In addition to heat resistance, PETG was chosen because it has high chemical resistance and toughness [73]. In terms of its mechanical properties, PETG lies between ABS and PLA [74]. PLA was ruled out as a filament because of the glass transition temperature of 60 °C [39] is too low to withstand thermal stress during the coating process. In addition, PLA loses its mechanical stability due to degradation processes [73].

2.3.1. Module 1: supply of filament

The development of module 1 included a gear housing (Fig. 2b) for the later filament supply, as well as a motor housing (Fig. 2d and e), in which a worm gear motor (Fig. 2c) (Miskall, Wuhan Papamao E-Commerce Co., Ltd., Wuhan, People's Republic of China) with matching gear pinions (Bondtech Drive Gear Kit 8 mm Welle, Bondtech, Värnamo, Sweden) was placed. Task of module 1 is providing filament. Due to the rotation speed of 12 rpm of the worm gear motor, a desired slow propulsion of the filament takes place for a later sufficient contact time of filament and nanomaterials for the surface melting in the copper tube of module 3. Filament is stored on shafts with ball bearings (Original Prusa i3 MMU2S Upgrade Kit, Prusa Research a.s., Czech Republic) mounted in filament spool holders (Fig. 2g), which were also printed and fastened in the motor housing.

Subsequent modules were always printed on already developed and assembled modules, whereby these were installed interlocking like stairs. For the following module 2 files were composed according to the completed module 1. With this file, the constructions of module 2 could be precisely adjusted to module 1. This procedure was also repeated for subsequent construction steps of module 3 and 4.

2.3.2. Module 2: Powdering of nanomaterials and merging with filament

Module 2 supplies nano-hydroxylapatit or nano-fluorapatite to PETG and PLA filament. Moisture from the surrounding environment led to aggregation of nanoparticles. Thereby, they reached sizes in the millimeter range, that made merging with filament impossible. For this reason, a sieve (Fig. 3a–c) and pestle (Fig. 3d) were designed, by which nHA or nFA were sieved and aggregations could be dissolved. The same filament was chosen as material for sieve insert and pestle as filament to be coated later. In this way, possible abrasion of pestle and sieve insert could not cause contamination of coated filament. As pestle and sieve insert needed a higher resolution, a printer nozzle with a diameter of 0.25 mm (nozzle fun pack, E3D-Online, United Kingdom) was used on another 3D printer (Original Prusa i3 MK3S +, Prusa Research a.s., Czech Republic).

The dissolved nanomaterial was passed into a stainless-steel funnel (Fig. 3k) (Exeqianming, Shenzen, People's Republic of China), which was attached to a funnel housing designed for this. In order to keep nanomaterial pourable in the interior of later modules, such as ptfe tube (MMU2S buffer ptfe tube, Prusa Research a.s., Czech Republic) and a further funnel, vibration was needed. Therefore, a total of six vibration motors (Sourcing Map DC 3 V–6 V, 32 mA, Asia Pacific Elite Ltd, People's Republic of China) was used. Rubber coating of these motors were removed to amplify vibration effects and enable suitable installation into parts manufactured later.
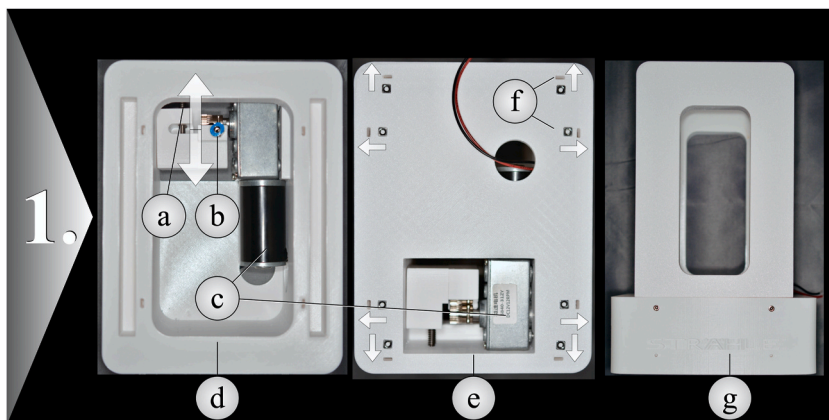

Fig. 2. Assembly of module 1
(a) coil springs (Prusa Research a.s., Czech Republic) enable forward and backward movements (see arrows) of the gear housing to compensate for production-related deviations of the filament diameter.
(b) filament supply via pfte tube (Prusa Research a.s., Czech Republic) and push-fit crew connection QSM-M5-4 (Festo Vertrieb GmbH & Co. KG, Germany)
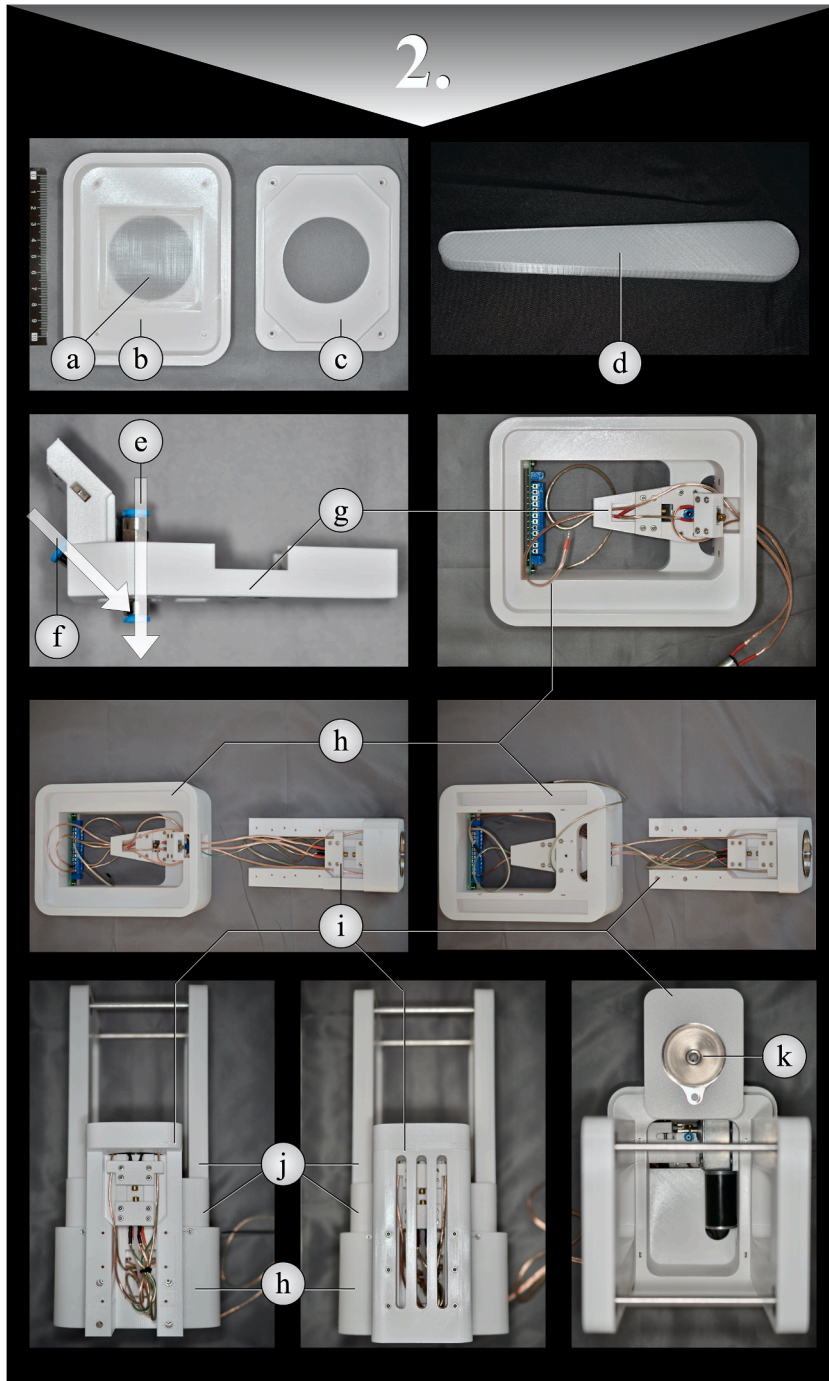(c) worm gear motor
(d) view from above on motor housing
(e) view from below on motor housinge
(f) 8 square nuts M3nS (Prusa Research a.s., Czech Republic) were inserted in the motor housing (see arrows). The square nuts served the stable fastening with module 2.
(g) filament spool holders mounted in motor housing.

(caption on next page)

Fig. 3. Assembly of module 2
(a) sieve insert made of ColorFabb_HT clear
(b) sieve bracket made of Prusament PETG signal white
(c) counter fixation for sieve bracket made of Prusament PETG signal white
(d) pestle made of ColorFabb_HT clear
(e) funnel cover with the course of the filament supplied later according to arrow
(f) funnel cover with the course of the nHA or nFA supplied later according to arrow
(g) funnel cover
(h) conneting housing
(i) funnel housing
(j) module 1
(k) stainless steel funnel for later added nHA or nFA in funnel housing.

During the cabling, braided copper speaker cables (Oehlbach Speaker Wire SP-7, Oehlbach Kabel GmbH, Germany) were used. Pure copper tolerates vibrations without increased susceptibility to cable breaks [75]. The cause of this is the plastic deformability of copper [75]. Nanomaterial trickled into another, smaller metal funnel (Koskerm GmbH, Germany), through which PETG or PLA filament (Fig. 3e) was supplied in the middle through a ptfe tube. In this way, both components were merged.

2.3.3. Module 3: surface melting of coated filament in order to incorporate nanomaterials

In Module 3, partial surface melting of PETG or PLA filament with nHA or nFA took place. Filament and nanopowder were merged in a 415 mm long copper tube (Fittingteile.de, Germany) with an inner diameter of 2 mm. Whereby heat was provided by two regulated peltier elements (Fig. 4h) (PTC heating elements AC DC 12 V, 220 °C, 5–28 W, Ovalat, People's Republic of China) and controlled via thermometer (Fig. 4l) (Weber 7581 Q Replacement Thermometer for Grills, Weber-Stephen Products LLC, U.S.A). The copper installation tube (Fig. 4i) was mounted vertically so that filament was not compressed or stretched after gravity. In this way, deviations in the filament diameter were minimized to increase print quality [41].

The copper tube was certified according to DIN EN 1057 for drinking water and heating installation. Therefore, it was expected that a passage of the filament through the pipe took place without contamination. The length of the copper tube was calculated based on the feeding speed of the filament, whereby a contact time of both components was carried out over a period of at least 60 s. Copper was chosen as the material because it has a high thermal conductivity [76].

Hereby, distributed nanomaterials were able to adhere to superficially heated filament. At the same time nanomaterials prevented an unwanted adhesion between filament and tube, as they formed an interfacial separating layer. The coating quantity could be regulated by manual additions of nHA or nFA. In the test phase, a maximum supply of nanopowder was established to determine maximal possible incorporation of nanomaterials on one hand and to avoid clogging of the tube on the other hand. For peltier elements, brackets printed with ColorFabb_HT clear (Fig. 4e) were manufactured because it withstands a permanent temperature load of 100 °C [63]. The copper tube was attached to a printed bracket with glass holders (Fig. 4f) (onpira GmbH, Germany), which in turn were attached to a module bracket (Fig. 4b). On their underside there were recesses (Fig. 4d) to mount stainless steel tubes (Fig. 4m) (H.-Hugo Brenschede GmbH, Germany) by which cable management took place. After cabling, module 2 was placed in the recess of module 3 and connected with four cylinder screws ISK M3X30 (MDG Service GmbH, Germany).

2.3.4. Module 4: base of coating machine

In addition to the base for connecting modules 1, 2 and 3 via stainless steel tubes (Fig. 5g), module 4 also includes a connection device for laboratory power supply units and a container to collect coated filament. There are two separate cable shafts in the base that run towards the frontal side. They serve for cable management of peltier elements (Fig. 5b) and motorization (Fig. 5c). The wiring passed through stainless steel tubes into the cable shafts of the base. The cables were installed on four banana plug sockets with a diameter of 4 mm (KUOQIY 4 mm banana plugs, Jincheng Qiyun Trading Co. Ltd., People's Republic of China) on the connection device for laboratory power supply units (Fig. 5i). Filament feeding and powder vibration were supplied with electricity via left banana plug sockets. For this purpose, three vibration motors were connected in series. Two of these series circuits were switched in parallel to the worm gear motor for filament feeding. In this way, a uniform, continuously adjustable voltage of 9–12 V could be provided for both operations, for filament feeding and vibration.

Banana plug sockets on the right provided power supply of both peltier elements. They were also switched in parallel. Due to the different connections an independent regulation of heat supply and filament feeding was possible. PETG or PLA filament coated with nHA or nFA cooled down by ambient air and could be harvested in a container (Fig. 5g) without contamination. The container (Fig. 5g) was printed with transparent Prusament PETG Clear (Prusa Research a.s., Prague, Czech Republic) (Table 1) to enable visual inspection of coated filament later. In the recesses for the hanging of the container (Fig. 5e) there was a square opening, of which filament could be later fed in an extruder of a 3D printer.

2.3.5. Initial commissioning and calibration of the filament coating machine

After final assembly, first peltier elements on the copper tube were checked for functionality. For this purpose, a laboratory power supply unit (Basetech BT-305, Conrad Electronic SE, Germany) was connected to banana plug sockets on the left side. A total of 10 series of measurements were carried out with different current intensities (Table 2). By this a suitable selection of current intensities was possible depending on the filaments used later. Since the temperature of the thermometer used ranged from 66 °C, temperatures
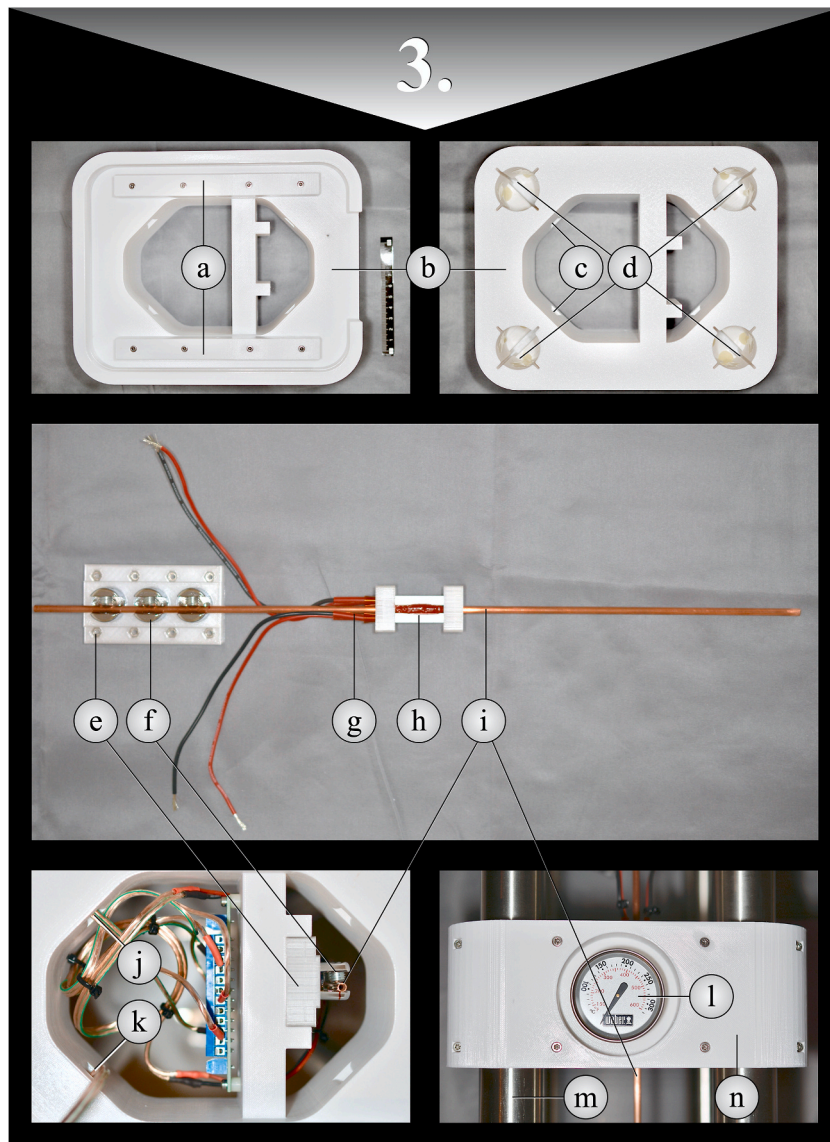
Fig. 4. Assembly of module 3
(a) module holder with anchoring elements for module 2
(b) module holder
(c) openings in module holder for cable management that flow into (d)
(d) recesses for stainless steel tubes
(e) mounting for copper tube, made of ColorFabb_HT clear
(f) glass holders
(g) power supply of peltier element
(h) peltier element
(i) copper tube
(j) power supply for peltier elements via right opening
(k) power supply for worm gear motor and vibration motors via left opening
(l) thermometer
(m) stainless steel tube
(n) mounting for thermometer.

were only recorded once this threshold was exceeded. All series of measurements from a current strength of 3.5 A had in common, that a temperature peak was reached after 270 s, which formed a plateau. For this reason, the time for reaching a constant temperature could be set to 300 s after the peltier elements were put into operation. Thereby, it could be ensured that a superficial fusion process of the filament with the added nanoparticles could take place. A current of 5.0 A with a target temperature of 100 °C was chosen for
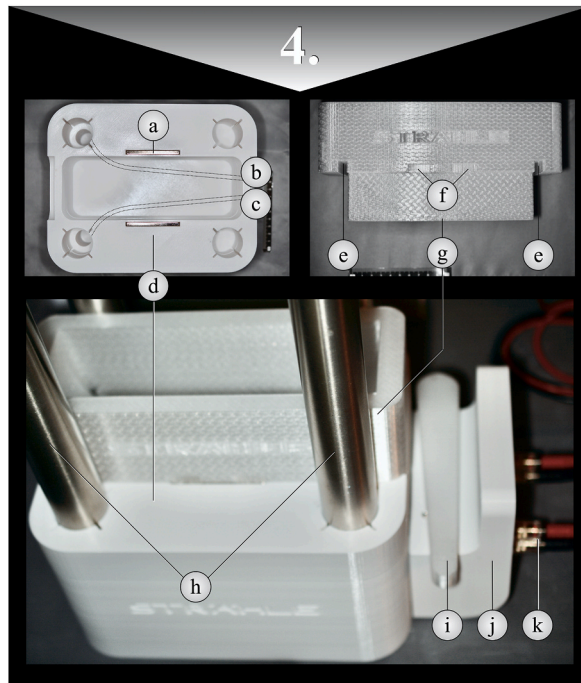
Fig. 5. Assembly of module 4
(a) neodymium magnet in base for later secure seating of the container
(b) shown course of wiring of peltier elements in base
(c) shown course of wiring for motorization in base
(d) base
(e) overhang of the container with printed recesses for frame-mounting on a 3D-printer
(f) cutouts for neodymium magnets for a later secure fit on base
(g) container
(h) stainless steel tubes
(i) pestle on the storage area of connection device for the laboratory power supplies
(j) connection device for the laboratory power supplies
(k) connected laboratory power supply with presets: 2.0 A and 12.0 V.

Table 2
Temperature increase of the peltier elements depending on the supplied current.

time in s	0	30	60	90	120	150	180	210	240	270	300
current in											
0,5 A	0 °C	0 °C	0 °C	0 °C	0 °C	0 °C	0 °C	0 °C	0 °C	0 °C	0 °C
1,0 A	0 °C	0 °C	0 °C	0 °C	0 °C	0 °C	0 °C	0 °C	0 °C	0 °C	0 °C
1,5 A	0 °C	0 °C	0 °C	0 °C	0 °C	0 °C	0 °C	0 °C	0 °C	0 °C	0 °C
2,0 A	0 °C	0 °C	0 °C	0 °C	0 °C	0 °C	0 °C	0 °C	0 °C	0 °C	66 °C
2,5 A	0 °C	0 °C	0 °C	0 °C	0 °C	0 °C	0 °C	0 °C	0 °C	66 °C	66 °C
3,0 A	0 °C	0 °C	0 °C	0 °C	0 °C	0 °C	0 °C	0 °C	66 °C	68 °C	68 °C
3,5 A	0 °C	0 °C	0 °C	0 °C	0 °C	0 °C	0 °C	66 °C	68 °C	70 °C	70 °C
4,0 A	0 °C	0 °C	0 °C	0 °C	0 °C	0 °C	66 °C	68 °C	70 °C	75 °C	75 °C
4,5 A	0 °C	0 °C	0 °C	0 °C	0 °C	66 °C	70 °C	75 °C	80 °C	85 °C	85 °C
5,0 A	0 °C	0 °C	0 °C	0 °C	66 °C	75 °C	83 °C	90 °C	95 °C	100 °C	100 °C

All values are rounded values. The ambient temperature was a constant 22 °C throughout the entire series of measurements.

coating of PETG while a current of 2.0 A was chosen for coating of PLA, as this allowed a constant temperature nearby measurable 66 °C to be achieved.

After testing the peltier elements, the filament feeding was tested with a PETG filament spool: For this purpose, a further laboratory power supply unit was connected to the right sockets with a voltage of 12 V and a current of 0.5 A. The left laboratory power supply unit providing the peltier elements was switched off. After filament passed through the copper tube, the power supply was briefly turned off to mark the protruding end of the filament with a waterproof universal pen (STAEDTLER Lumocolor® Pen 313, STAEDTLER Mars GmbH & Co. KG, Germany). This was followed by commissioning lasting 60 s, after which the power supply was briefly

interrupted again and the filament was marked. In total, this process was repeated ten times and each section was measured (Table 3), with the average being 415 mm. During operation, vibrations were tactilely noticeable in the area of the sieve holder and the funnel housing due to the vibration motors, which were also powered via this connection.

A second test run lasting 30 min was then carried out, in which the peltier elements were additionally supplied with a voltage of 12 V and a current of 5 A, resulting in a temperature of 100 °C. After 30 min, the total length of the filament was determined to be 12,300 mm. The average measurement of the filament path was 410 mm. This was 5 mm less than without the peltier elements switched on. Friction on the heated copper tube could be responsible for that, although this effect could be reduced by adding nHA or nFA later. The intended contact time of 60 s could be achieved regardless if peltier elements were put in operation or not.

2.4. Production of filament with and without coating

First, uncoated PETG or PLA filament was harvested. Therefore, the following steps were carried out: inserting a filament spool of PETG, filament feeding with interruption and removal of already passed filament, filament feeding for 900 s, interruption of filament feeding, cutting of and storage of harvested filament and removal of the spool (Table 4). For this purpose, PETG filament was cut off at the end of the copper tube with a pair of pliers (KNIPEX pliers 99 00 280, KNIPEX-Werk, Germany). PETG filament harvested was then placed in a labeled, resealable and food-safe all-purpose bag (Toppits® Zipper® all-purpose bag, 3 l, Cofresco Frischhalteprodute GmbH & Co. KG, Germany). Afterwards the container was cleaned with a sterile gauze swab (Medrull Gauze swabs sterile 10 cm × 10 cm, FORANS International AG, Switzerland) soaked in isopropyl alcohol (Maxxi Clean - Gabriela Baumgarten, Germany) for 90 s to remove particles created by abrasion. In order to be able to remove the PETG filament spool, the polarity had to be reversed. After 120 s there was no filament between gears, and removal from the spool holder was possible.

A series of tests with uncoated PLA filament was then carried out in the same way (Table 4). PETG and PLA filament served as control group for later examinations, such as possible contaminations during filament advancement due to abrasion of gears, as well as friction when passing through the ptfe hose elements, push-in fittings, metal funnels and copper tubes.

In order to coat PETG filament with nano-hydroxyapatite, the workflow was expanded by the use of sieves and pestles, weighing and sieving of nHA, as well as switching the peltier elements on and off (Table 4). The sieve insert for this series of tests was also made of PETG, just like the pestle. Using a sterile cement spatula (HS cement spatula wide, Henry Schein Inc., U.S.A.) and a bench scale (Beurer type KS 19 Fresh, Beurer GmbH, Germany), a total of 4 g of nano-hydroxyapatite powder was added to the sieve in 1 g portions. While nano-hydroxyapatite powder was added, nitrile examination gloves were worn as protection against contamination. After each powder addition, agglomerated nano-hydroxyapatite particles were pressed through the sieve with a mesh width of 0.26 mm using a pestle to produce smaller powder particles. These became even smaller as vibration continued. Filament, which was coated within 300 s, was separated from the end of the copper tube using wipe-disinfected pliers. This strand was discarded. An incorporation of hydroxyapatite powder particles on the surface of the rejected strand would only be expected towards the end of 300 s when a temperature of 100 °C was reached. In the period of time before reaching 100 °C, filament surface was not heat enough and, therefore, not receptive to nHA particles. After reaching 100 °C, PETG filament coated with nHA for 900 s was harvested. After 900 s, coated PETG filament was cut off at the end of the copper tube using a pair of pliers. Then the power supply of the peltier elements was switched off. The filament feeding remained in operation for another 300 s until the copper tube had cooled down. This prevented unwanted adhesion of filament to the hot copper tube. After 300s the filament strand was also discarded. In total, around 6 m of PETG filament coated with nHA were harvested. An exact measurement was not carried out to avoid contamination, unwanted removal of only partially incorporated powder particles and twisting during unwinding.

For the test series of PLA filament with nHA, steps of the procedure (Table 4) were repeated as described for PETG filament coated with nHA. Any nHA remaining in the coating machine from previous series of PETG did not need to be removed. However, due to abrasion, sieve insert and pestle made of PLA were used. Furthermore, the temperature of the peltier elements was adjusted to PLA.

After coating PLA, the filament coating machine was cleaned to remove remaining nano-hydroxyapatite residues (Fig. 6). These would otherwise have led to mixing in further series of tests with nano-fluoroapatite. After removing the sieve holder, the exposed stainless-steel funnel (Fig. 3k) was cleaned with a vacuum cleaner (Miele vacuum cleaner Classic C1 EcoLine, Miele

Table 3
Measurement of the filament path in sections.

time	total distance in mm	distance in mm after 60 s
60 s	412	412
120 s	826	414
180 s	1242	416
240 s	1657	415
300 s	2073	416
360 s	2488	415
420 s	2903	415
480 s	3319	416
540 s	3736	417
600 s	4150	414
average distance traveled per minute in mm		415
SD (standard deviation) in mm		1.304

Table 4
Workflow for coated and uncoated filaments.

work steps	PETG (control group)	PLA (control group)	PETG + nHA	PLA + nHA	PETG + nFA	PLA + nFA
1.	insert filament spool (colorFabb_HT clear, 1.75 mm, colorFabb B.V., Netherlands)	inserting filament spool (extrudr PLA NX2 white, Extrudr FD3D GmbH, Austria)	insert filament spool (colorFabb_HT clear, 1.75 mm, colorFabb B.V., Netherlands)	inserting filament spool (extrudr PLA NX2 white, Extrudr FD3D GmbH, Austria)	insert filament spool (colorFabb_HT clear, 1.75 mm, colorFabb B.V., Netherlands)	inserting filament spool (extrudr PLA NX2 white, Extrudr FD3D GmbH, Austria)
2.	–	–	insert sieve (sieve insert and pestle each made from newly manufactured PETG)	insert sieve (sieve insert and pestle each made from newly manufactured PLA)	insert sieve (sieve insert and pestle each made from newly manufactured PETG)	insert sieve (sieve insert and pestle each made from newly manufactured PLA)
3.	–	–	usage of a total of 4g nHA (Kalident Powder 100 1ST B (17 kGy), Kalichem srl, Italy) in portions with sterile cement spatula, nitrile examination gloves and bench scales; seven from nHA	usage of a total of 4g nHA (Kalident Powder 100 1ST B (17 kGy), Kalichem srl, Italy) in portions with sterile cement spatula, nitrile examination gloves and bench scales; seven from nHA	usage of a total of 4g nFA (Charge: RC2206379; S&C Polymer GmbH, Germany) in portions with sterile cement spatula, nitrile examination gloves and bench scales; seven from nFA	usage of a total of 4g nFA (Charge: RC2206379; S&C Polymer GmbH, Germany) in portions with sterile cement spatula, nitrile examination gloves and bench scales; seven from nFA
4.	–	–	turn on peltier elements (U = 12 V, I = 5 A)	turn on peltier elements (U = 12 V, I = 5 A)	turn on peltier elements (U = 12 V, I = 5 A)	turn on peltier elements (U = 12 V, I = 5 A)
5.	filament feeding for t = 120 s (U = 12 V, I = 0.5 A)	filament feeding for t = 120 s (U = 12 V, I = 0.5 A)	filament feeding for t = 120 s (U = 12 V, I = 0.5 A)	filament feeding for t = 120 s (U = 12 V, I = 0.5 A)	filament feeding for t = 120 s (U = 12 V, I = 0.5 A)	filament feeding for t = 120 s (U = 12 V, I = 0.5 A)
6.	stop filament feeding (U = 0 V, I = 0 A)	stop filament feeding (U = 0 V, I = 0 A)	stop filament feeding (U = 0 V, I = 0 A)	stop filament feeding (U = 0 V, I = 0 A)	stop filament feeding (U = 0 V, I = 0 A)	stop filament feeding (U = 0 V, I = 0 A)
7.	–	–	control target temperature: 100 °C	control target temperature: 66 °C	control target temperature: 100 °C	control target temperature: 66 °C
8.	separation and discarding of filament after passage through copper tube	separation and discarding of filament after passage through copper tube	separation and discarding of filament after passage through copper tube	separation and discarding of filament after passage through copper tube	separation and discarding of filament after passage through copper tube	separation and discarding of filament after passage through copper tube
9.	filament feeding for t = 900 s (U = 12 V, I = 0.5 A)	filament feeding for t = 900 s (U = 12 V, I = 0.5 A)	filament feeding for t = 900 s (U = 12 V, I = 0.5 A)	filament feeding for t = 900 s (U = 12 V, I = 0.5 A)	filament feeding for t = 900 s (U = 12 V, I = 0.5 A)	filament feeding for t = 900 s (U = 12 V, I = 0.5 A)
10.	stop filament feeding (U = 0 V, I = 0 A)	stop filament feeding (U = 0 V, I = 0 A)	stop filament feeding (U = 0 V, I = 0 A)	stop filament feeding (U = 0 V, I = 0 A)	stop filament feeding (U = 0 V, I = 0 A)	stop filament feeding (U = 0 V, I = 0 A)
11.	separation of filament after passage through the copper tube	separation of filament after passage through the copper tube	separation of filament after passage through the copper tube	separation of filament after passage through the copper tube	separation of filament after passage through the copper tube	separation of filament after passage through the copper tube
12.	separation of filament after passage through the copper tube and storage of PETG filament in 3l all-purpose bag; cleaning of container	separation of filament after passage through the copper tube and storage of PLA filament in 3l all-purpose bag; cleaning of container	separation of nHA coated filament after passage through the copper tube and storage of PETG filament in 3l all-purpose bag; cleaning of container	separation of nHA coated filament after passage through the copper tube and storage of PLA filament in 3l all-purpose bag; cleaning of container	separation of nFA coated filament after passage through the copper tube and storage of PETG filament in 3l all-purpose bag; cleaning of container	separation of nFA coated filament after passage through the copper tube and storage of PLA filament in 3l all-purpose bag; cleaning of container
13.	–	.	switching off peltier elements and stop filament feeding for t = 300 s (U = 12 V, I = 0.5 A)	switching off peltier elements and stop filament feeding for t = 300 s (U = 12 V, I = 0.5 A)	switching off peltier elements and stop filament feeding for t = 300 s (U = 12 V, I = 0.5 A)	switching off peltier elements and stop filament feeding for t = 300 s (U = 12 V, I = 0.5 A)
14.	return of filament for 120 s by reversing the polarity (U = 12 V, I = 0.5 A)	return of filament for 120 s by reversing the polarity (U = 12 V, I = 0.5 A)	return of filament for 120 s by reversing the polarity (U = 12 V, I = 0.5 A)	return of filament for 120 s by reversing the polarity (U = 12 V, I = 0.5 A)	return of filament for 120 s by reversing the polarity (U = 12 V, I = 0.5 A)	return of filament for 120 s by reversing the polarity (U = 12 V, I = 0.5 A)
15.	removing filament spool	removing filament spool	removing filament spool	removing filament spool	removing filament spool	removing filament spool
16.	–	–	–	cleaning powder feed with vacuum cleaner and round wire	–	cleaning powder feed with vacuum cleaner and round wire

Fig. 6. Cleaning of the coating machine for filament
(a) sieve bracket made of Prusament PETG signal white
(b) laterally distributed powder of nHA
(c) sieve insert made of ColorFabb_HT clear
(d) orthodontic wire
(e) ColorFabb_HT clear
(f) stainless steel funnel for previously added nHA in funnel housing.

Vertriebsgesellschaft Deutschland KG, Germany) at the highest level for 60 s. In addition, further mechanical cleaning was carried out using orthodontic wire (Central Iron and Steel Research Institute, Orthodontic Wire, 0.45 mm, People's Republic of China). Both types of cleaning were carried out alternately five times each.

To obtain the test series of PETG filament coated with nano-fluorapatite, steps of the procedure (Table 4) were carried out as for coating of PETG filament with nHA. Instead of using nHA a total of 4g nFA was used. For the test series of PETG filament coated with nFA, a new unused sieve insert and pestle made of PETG were used. The sieve insert and pestle previously used for nHA were no longer applied so that in the event of possible abrasion of the materials during sieving, only particles made of PETG filament and none of nHA ended up in the admixture.

A newly manufactured sieve insert and pestle made of PLA were also used to coat PLA filament with nFA. Settings for the remaining work steps were identical in their execution to the previously described work steps for coating PLA with nHA (Table 4). The powder supply systems were cleaned after PLA coating. Here too, the procedure was identical to that carried out after producing PLA coated with nHA.

2.5. Determining diameters of coated and uncoated filament

From all test series, 1000 mm long pieces of filament were cut off, which were then divided into ten 100 mm long pieces. This should prevent the filament from coiling, which happens if the thread strand is longer than approximately 600 mm. Coiled filament would have falsified the measurement results due to kinks or bends. To avoid contamination with dust from the environment or sodium chloride of the finger tips, new nitrile examination gloves were worn for each filament test series. Additionally, the pair of pliers were cleaned with sterile gauze swabs soaked in 99.9 % isopropanol for 90 s before each cut of a new filament test series.

The diameter measurement was taken at the center of each of the 100 mm long filament pieces. The alignment of the filament was determined using dental loupes (DCI flip-up Classic 2.5x with LED light HighlightR, DCI - Dental Consulting GmbH, Germany). One side showed impressions and had indentations from the gears from filament feeding, while the remaining circumference of the filament appeared smooth. Two sides were always alternately positioned between the measuring anvil and the measuring spindle of a micrometer (Mitutoyo item no. 103–129; Mitutoyo, Japan): To measure the first piece of filament, the diameter was determined on the side on which impressions of gears were visible. The second piece of filament was measured on smooth surfaces at an angle of 90° to gear impressions. The measurements were repeated alternately a total of 10 times as described. As soon as the measuring spindle came into contact with the filament, the ratchet stop made three rotations. For each new series of filament, the measuring anvil and measuring spindle were cleaned to remove possible powder residues by using sterile gauze swabs soaked in 99.9 % isopropanol for 90 s.

2.6. Printing test specimens from coated and uncoated filament

In order to compare printing quality and material properties of uncoated and coated filament made of PETG or PLA, test specimens were printed in the form of cubes, whereby the maximum possible base area of one cube was determined by the diameter of the holders for the SEM of 12.7 mm (SEM pin stub, ø 12.7 mm, Micro to Nano, Netherlands). This resulted in an edge length of 9.00 mm, allowing examination of different cube surfaces by rotating to examine different printed structures. A total of three cubes were printed per

filament, each of which had a different surface examined: a top surface (Fig. 7e), a side surface with a fold and another adjacent side surface (Fig. 7f).

To print three cubes two G-codes (Table 5) were created, one for PETG and one for PLA. The infill was 80 % in each case. As the filament had been already coated, the settings for the G-codes were based on the respective carrier filament used. No separate adjustment was made based on the usage of coatings or on the usage of coated or uncoated filaments. However, adjustments werde made based on usage of PETG or PLA. The prints were carried out with an extrusion printer, modified with a 0.25 mm nozzle. By printing three cubes each, the suitability of filaments for a longer printing time of 125 min was tested. Additionally, suitability for accuracy and reproducibility of structures were tested using a 0.25 mm printing nozzle and 0.5 mm high printing layers. Grid was chosen as the infill type as it is printed in both directions. This means that the nozzle of the printer is guided over intersections of the infill. This could lead to print interruptions with filament with large diameter fluctuations, as the nozzle can get stuck at crossing points due to extrusion excesses. By choosing grid as infill type, the printability of the filament could be examined in this way.

Different steps were necessary to print test specimens made of uncoated PETG filament (Table 5). Previously harvested PETG filament was placed in the container mounted on the printer frame. A filament change was then carried out. After 1800 s, printing was interrupted and test specimens that had already been printed were discarded. This was due to remaining filament in the extruder from previous prints, which mixes in the initial phase of printing until it is used. However, this unwanted admixture would have led to contamination. After that a new printing process was performed to produce test specimens. These were removed using nitrile examination gloves and stored in a labeled 3-L all-purpose bag afterwards. The printing sheet was then cleaned of printing residues according to the manufacturer's instructions. Possible particles were removed from the PETG filament in the container and on the extruder using a sterile gauze swab soaked in 99.9 % isopropanol. In addition to using a different printing sheet and cleaning, the work processes (Table 5) for producing the test specimens from PLA corresponded to those previously described for PETG filament.

The workflow for producing test specimens from PETG filament with nano-hydroxylapaptite or nano-fluorapatite coating was identical to the workflow for producing test specimens from PETG filament. The only difference was the presence of the added nanomaterials. The production of test specimens from PLA filament with nano-hydroxylapaptite or nano-fluorapatite coating was also identical to the workflow for the production of test specimens from PLA filament.

2.7. Preparation of samples for examination and analysis with the SEM

In order to show differences in the powder admixtures and to enable comparison with the later coatings, a powder sample of nHA and nFA was prepared for the SEM. A plate prepared with an adhesive pad (EM-Tec CT 12, Micro to Nano, Netherlands) was pressed into nHA or nFA and then tapped off.

As for diameter measurement before, 1000 mm long pieces were cut off from remaining filament residues, with pair of pliers being cleaned with a sterile gauze swab soaked in 99.9 % isopropanol for 90 s for each new filament test series. The piece of filament was divided into thirds. These thirds were each attached to an SEM sample plate with an adhesive pad, with adhesion achieved by pressing on protruding ends, which were then removed. Three pieces of filament were produced for each series of experiments.

Previously printed test specimens were attached to plates using adhesive pads. For each test specimen, a different surface of the cube was selected, each facing upwards. Thereby, differences in surface morphology caused by extrusion printing and used filaments could later be shown in the SEM.
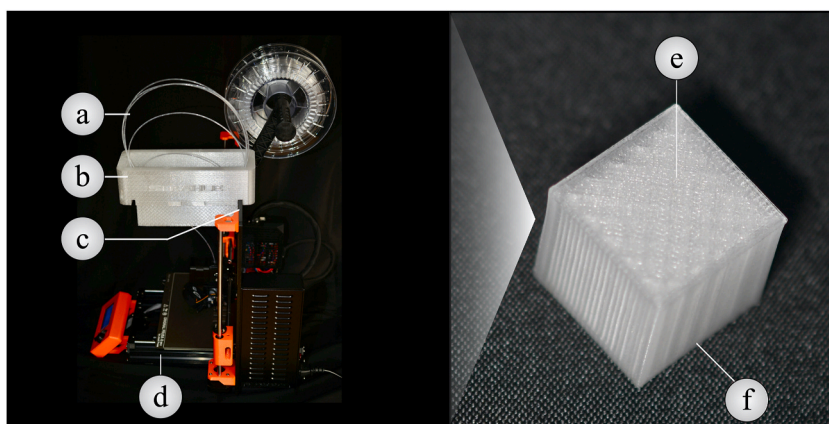

Fig. 7. Printing test specimen with coated filament
(a) ColorFabb_HT clear (PETG) coated with nHA
(b) container
(c) fastening the container to the frame
(d) Original Prusa i3 MK3s + 0.25 nozzle
(e) top surface of cube printed with nHA coated PETG
(f) side surface top surface of cube printed with nHA coated PETG.

Table 5
Production of test specimen.

Work order	Work process	Special features for	
		PETG, PETG + nHA, PETG + nFA	PLA, PLA + nHA, PLA + nFA
1.	used filament as carrier material	colorFabb_HT clear, 1.75 mm (colorFabb B.V., Netherlands)	extrudr PLA NX2 white (Extrudr FD3D GmbH, Austria)
2.	mount suitable printing sheet (Prusa i3 MK3s+)	double-sided textured PEI powder-coated spring steel sheet for Original Prusa i3 MK3/S/+ and MK2.5/S heatbeds (Prusa Research a.s., Czech Republic)	spring steel sheet with smooth double-sided PEI for the Original Prusa i3 MK3/S and MK2.5/S heatbeds (Prusa Research a.s., Czech Republic)
3.	place the filament in container using nitrile examination gloves	PETG, PETG + nHA,	PLA, PLA + nHA,
4.	mount collection container on the printer frame (Prusa i3 MK3s+)	PETG + nFA	PLA + nFA
5.	change of filament (Prusa i3 MK3s+)		
6.	print test specimens for 1800 s, then stop the printing process and discard the test specimens		
7.	print test specimen with following printing parameters	Original Prusa i3 MK3s + 0.25 nozzle	Original Prusa i3 MK3s + 0.25 nozzle
	nozzle temperature	270 °C	205 °C
	heatbed temperature	100 °C	60 °C
	number of perimeters	3	3
	top solid layers	8	8
	bottom solid layers	8	8
	layer thickness	0.05 mm	0.05 mm
	fill density	80 %	80 %
	infill type	grid	Grid
	supports	none	none
	printing time	7500 s	7500 s
8.	cooling of printing sheet		
9.	remove the test specimen using nitrile examination gloves, storage of the test specimens	store in separate 3 l general purpose bags	store in separate 3 l general purpose bags
10.	clean printing sheet	sterile gauze pad, soaked in water and dish soap	sterile gauze pad, soaked in 99.9 % isopropanol
11.	removal of remaining filament from container		
12.	clean container and extruder	sterile gauze pad, soaked in 99.9 % isopropanol	sterile gauze pad, soaked in 99.9 % isopropanol

All samples to be examined did not have sufficient conductivity for direct observation with the SEM, thus sputtering with gold was necessary [77]. Without sputtering, non-conductive samples become charged when scanned with the electron beam in the SEM [77]. Two coating processes, each lasting 35 s, were carried out (Balzers SCD 030, BAL-TEC AG, Liechtenstein). A longer total duration would have caused undesired thermoplastic changes to the test specimen and filament samples and would have covered the thin powder layer of nHA or nFA, which would no longer have made analysis possible. In order to further increase the conductivity of printed test specimens, four side surfaces were covered with conductive SEM aluminum adhesive tape (EM-Tec conductive SEM aluminum adhesive tape, Micro to Nano, Netherlands).

All samples on SEM plates were stored dust-protected before and after SEM examination in a printed box with suitable recesses for SEM pin plates and an associated lid. In addition, the box was placed in a 3-L all-purpose bag and sealed airtight with the ziplock. The all-purpose bag was only opened to remove samples and test specimens from the box.

2.8. Visualization of surfaces with SEM

All samples were examined with an SEM (XL 30 ESEM FEG, FEI, Netherlands). Where possible, images of the sample surface were obtained using a Secondary Electrons (SE) detector, as the electron emissions offer high resolution [78].

However, charging phenomena sometimes occurred. To prevent this, the operating voltage can be reduced [77]. In the present study, this was not done for the samples so that a uniform operating voltage of 10 kV should ensure comparability. Instead a back-scattered electrons (BSE) detector was chosen for image creation when charging phenomena occurred: This detects deflected electrons from the primary beam, which, however, leads to a lower resolution than SE radiation [78]. SE detectors and BSE detectors can also be used together to obtain images of sample surfaces [79]. If less charging phenomena occurred, this image acquisition was preferred to pure BSE image presentation in this work. The surface morphology of nHA and nFA powder was examined under a magnification of 500 to 20,000 times, of filament test series under a magnification of 50 to 1000 times if possible and of test specimens under a magnification of 250 to 2000 times.

2.9. Analysis of the mass proportions of powder, filament and test specimens

In addition to the surface analysis, mass fractions of all samples were also analyzed to gain information about elements caused by

coating and possible contamination. A mass fraction analysis is possible by measuring X-rays emitted by an element in the preparation using a focused electron beam [80]. In SEM, this procedure is called EDX [81]. The SEM used a detector with corresponding software (EDX Multi-Element Mapping, Version 3.35, EDAX INC., Ametek, U.S.A.). First, a section of the surface to be examined was selected. Within the respective test series, this section was kept as constant as possible in size and position in order to ensure comparability. An analysis was carried out at 10 kV for 120 s each, with the mass fraction Wt% (Weight Percent) being recorded for each element occurring in the object.

3. Results

3.1. Nanomaterials

Nano-hydroxyapatite powder (Fig. 8a) and nano-fluorapatite powder (Fig. 8b) were examined by SEM for morphology and composition. Smallest particle sizes of nHA were approximately 200 nm (Fig. 8a), while for nFA these were 50 nm (Fig. 8b).

In the EDX analysis, the mass fraction of oxygen in nHA was 30.76 % and in nFA 32.22 %, that of phosphorus in nHA was 12.16 % and in nFA 15.11 % and that of calcium in nHA was 23.89 % and at nFA 32.48 %. Hydrogen, which is contained in nHA, for example, cannot be detected with EDX and, therefore, is not discussed further. The remaining mass fractions gold, nitrogen and carbon were contained due to sputtering.

Nano-fluorapatite powder also contained Fluorine at 3.58 %. However, there were two special features with nFA: On the one hand, the sample charged in the SEM, which meant that observation was only possible in a mix of SE and BSE detectors. On the other hand, the sample also contained 0.98 % sodium.

3.2. Coated and uncoated filament

Uncoated filaments served as control, because surface morphology did not undergo surface treatment as in the coating process. Due to the high charges on the samples (Fig. 9a and c), images with PETG were only possible at a maximum magnification of 250×. Surface of PETG filament was smooth (Fig. 9a), which was interrupted by indentations perpendicular to the longitudinal axis (Fig. 9a arrow) at a distance of approximately 500 μm from impressions of the gear. Using EDX, a mass fraction of carbon between 50.93 % and 54.21 % (Table 5) and of oxygen between 30.75 % and 32.39 % (Table 6) could be detected in all PETG filaments.

With PLA, images with an SE detector could be performed at a magnification of up to 1,000×. The surface texture of PLA filament appeared rough (Fig. 9b–d, e, f) with varying levels of deposits on the filament of up to 40 μm (Fig. 9e). As with PETG, indentations perpendicular to the longitudinal axis were also visible in PLA (Fig. 9b), which were caused by gears. However, they were not as noticeable in depth. Mass fraction for PLA varied, such as carbon from 32.23 % to 33.20 % (Table 6), and oxygen from 45.43 % to 48.10 % (Table 6). In addition, calcium was detected with a mass fraction of 4.71 %–7.09 % (Table 6), which was therefore responsible for the white color. Apart from gold and nitrogen for the coating process of the samples, no other elements were analyzed for PLA or PETG.

SEM observations of filaments coated with nanomaterial were intended to provide information, whether deagglomeration and incorporation of nanoparticles on the filament surface had occurred and to what extent the surface morphology of the filament had changed due to powder admixture and heat treatment.
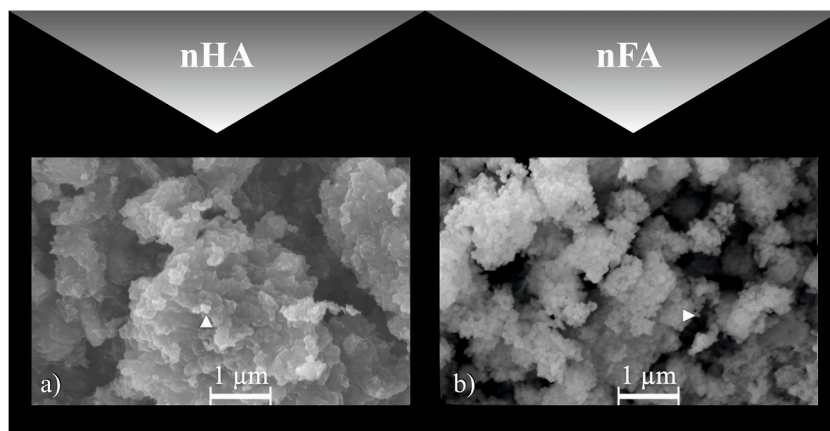

Fig. 8. SEM images of used nanomaterials
(a) nano-hydroxyapatite: magnification 20,000×:
▲ points to the smallest nHA particles with a size of 200 nm
(ss) nano-fluorapatite: magnification 20,000×:
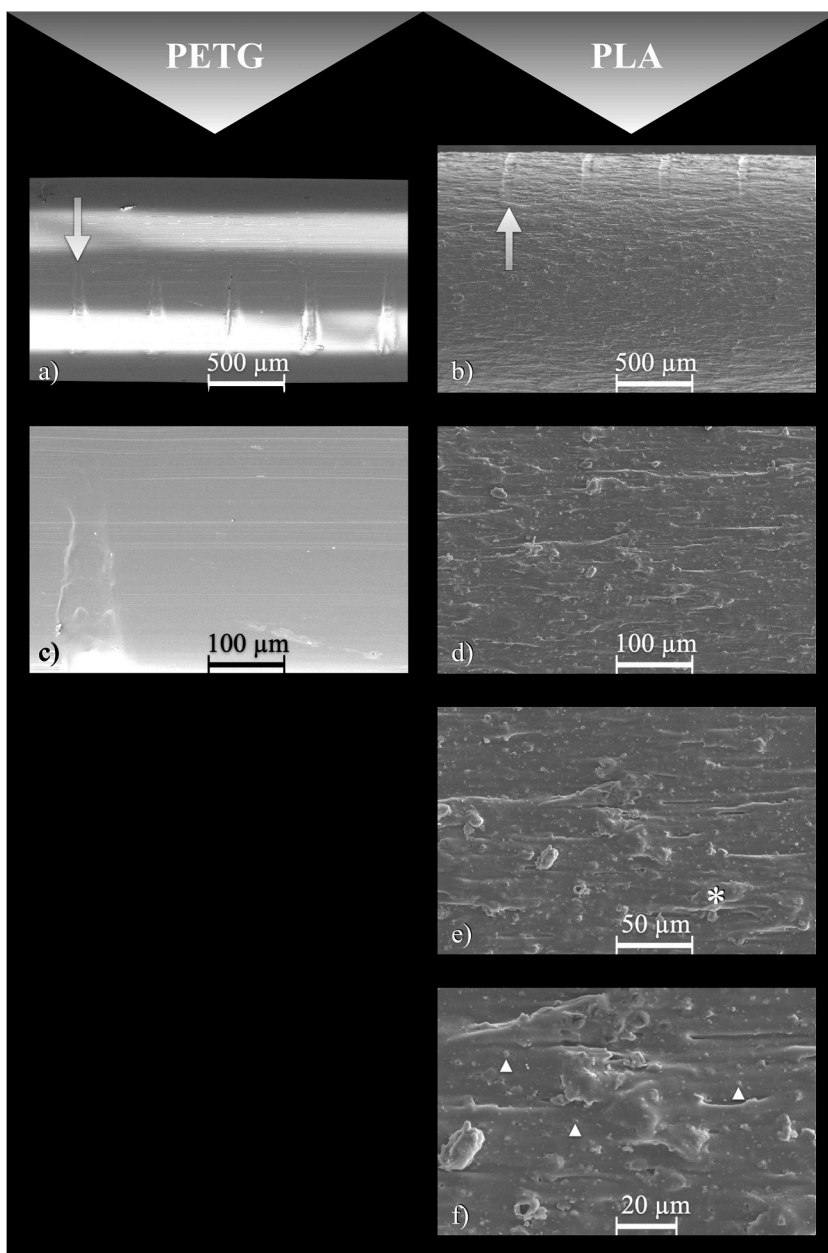▶ points to the smallest nFA particles with a size of 50 nm.

Fig. 9. SEM images of uncoated PETG and uncoated PLA filament
(a) uncoated PETG filament: magnification 50×
white arrow points to one of several notches
(b) uncoated PLA filament: magnification 50×
white arrow points to one of several notches
(c) uncoated PETG filament: magnification 250×
(d) uncoated PLA filament: magnification 250×
(e) uncoated PLA filament: magnification 500×
* points to production-related elevation with a size of 40 μm
(f) uncoated PLA filament: magnification 1,000×
▲ points to calcium particles with sizes of 2–5 μm.

As with the control group (Fig. 9a–c), the PETG filament with nHA showed smooth surfaces (Fig. 10a–c, e, g) that were covered with a thin, irregularly distributed nHA powder layer. Accumulations of nHA were visible at the indentations created by the gears (Fig. 9a arrow). The smallest nHA particles had a size of approximately 200 nm (Fig. 10e), which appeared to be incorporated because they did

Table 6

Mass fractions of coated and uncoated filaments in wt%.

Sample	A01	A02	A03	E01	E02	E03	B01	B02	B03	F01	F02	F03	C01	C02	C03	G01	G02	G03
Elements	PETG	PETG	PETG	PLA	PLA	PLA	PETG + nHA	PETG + nHA	PETG + nHA	PLA + nHA	PLA + nHA	PLA + nHA	PETG + nFA	PETG + nFA	PETG + nFA	PLA + nFA	PLA + nFA	PLA + nFA
C	51.62	54.21	50.93	32.23	32.74	33.20	53.51	50.72	53.85	23.11	16.53	20.40	52.31	44.79	50.07	18.90	18.41	30.53
N	3.41	2.77	4.34	2.78	2.17	3.03	2.82	3.78	3.78	3.64	3.96	3.16	3.77	3.87	3.56	3.89	4.51	3.61
O	30.75	31.09	32.39	45.43	46.49	48.10	29.67	30.87	31.40	44.43	40.88	42.72	30.55	31.08	31.75	40.93	38.31	45.35
F								1.04					1.28	1.27	1.49	2.48	2.87	0.78
Na								0.41					0.54	0.16	0.35	0.70	0.87	0.35
P							1.31	0.71	1.21	4.87	7.51	5.87	1.35	2.74	1.44	6.98	7.09	1.67
Au	14.23	11.93	12.34	12.47	12.64	10.96	10.17	11.06	7.11	14.14	12.16	11.52	7.81	10.72	8.41	13.43	13.50	13.62
Ca				7.09	5.96	4.71	2.52	1.41	2.65	9.80	18.95	16.33	2.39	5.38	2.93	12.67	14.45	4.09

Note: Percentages represent mass fractions (Wt%). Values are rounded.

Abbreviations: Carbon (C), Nitrogen (N), Oxygen (O), Fluorine (F), Sodium (Na), Phosphorus (P), Gold (Au), Calcium (Ca).
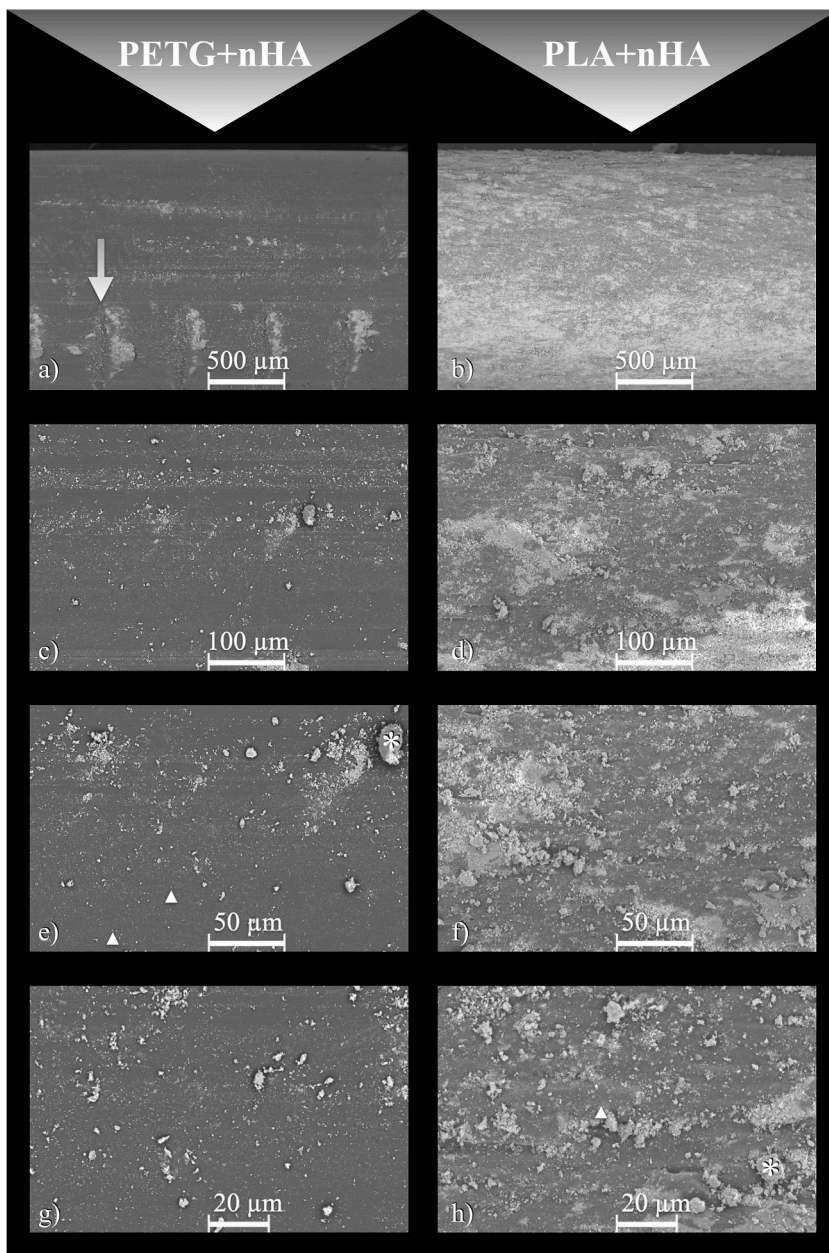
Fig. 10. SEM images of nHA coated PETG and nHA coated PLA filament

a) nHA coated PETG filament: magnification 50×

white arrow points to one of several notches and nHA powder deposits

b) nHA coated PLA filament: magnification 50×

c) nHA coated PETG filament: magnification 250×

d) nHA coated PLA filament: magnification 250×

e) nHA coated PETG filament: magnification 500×

▲ points to smallest nHA particles with sizes of 200 nm

* points to agglomerated nHA particles with a size of 25 μm

f) nHA coated PLA filament: magnification 500×

g) nHA coated PETG filament: magnification 1,000×

h) nHA coated PLA filament: magnification 1,000×

▲ points to smallest nHA particles with sizes of 200 nm

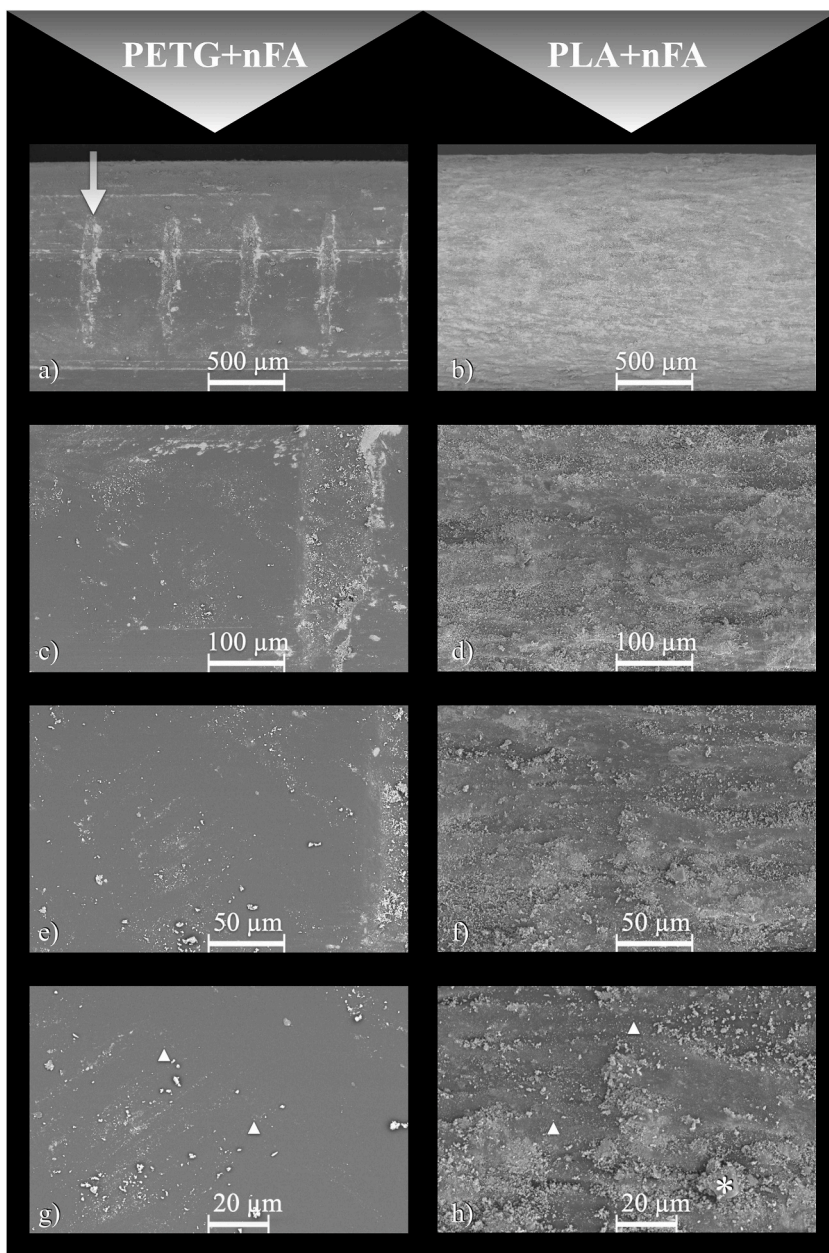* points to agglomerated nHA particles with a size of 7,5 μm.

Fig. 11. SEM images of nFA coated PETG and nFA coated PLA filament

a) nFA coated PETG filament: magnification 50×

white arrow points to one of several notches and nFA powder deposits

b) nFA coated PLA filament: magnification 50×

c) nFA coated PETG filament: magnification 250×

d) nFA coated PLA filament: magnification 250×

e) nFA coated PETG filament: magnification 500×

f) nFA coated PLA filament: magnification 500×

g) nFA coated PETG filament: magnification 1,000×

▲ points to smallest nFA particles with sizes of 100 nm

h) nFA coated PLA filament: magnification 1,000×

▲ points to smallest nFA particles with sizes of 100 nm

* points to agglomerated nFA particles with a size of 15 μm.

not change position during the scanning process.

The EDX analysis showed a mass fraction of carbon of 50.72 %–53.85 % for PETG (Table 6) and of 29.67 %–31.40 % for oxygen (Table 6). Another focus was on determining the admixture of nHA. Since oxygen has already been assigned in the analysis of PETG, the consideration was limited to components contained only in nHA, such as phosphorus with mass fractions of 0.71 %–1.31 % (Table 6) and calcium of 1.41 % up to 2.65 % (Table 6). Sample B02 contained fluorine in a mass fraction of 1.04 % (Table 6) and sodium in a fraction of 0.41 % (Table 6), which were not contained in either nHA or PETG.

When looking at the surface morphology of PLA filament coated with nHA, production-related unevenness had reduced in size to 7,5 μm (Fig. 10h*). At the same time, there was a varying degree of distribution of particles (Fig. 10b–d, f, h). Impressions of gears were only visible in filament sample F01, while these were not visible in other samples, because they were glued to the impressions caused by gears.

Mass fractions of surface composition were determined using EDX. For test specimen F02 (Table 6), the dimensions of the examined section did not correspond to those of the other test specimens. The proportion of carbon for PLA coated with nHA was 16.53 %–23.11 % (Table 6) and for oxygen it was 40.88 %–44.43 % (Table 6). Since mass fraction of oxygen has already been assigned to PLA, here, as with nHA-coated PETG, a limited analysis is carried out on mass fractions contained only in nHA, such as phosphorus and calcium. Phosphorus could be detected with a mass fraction of 4.87 %–7.51 % (Table 6) and calcium with a mass fraction of 9.80 %–18.95 % (Table 6). In addition to gold and nitrogen for the coating process of the samples, no other elements were identified in both PLA or PETG coated with nHA.

Nano-fluorapatite coated PETG filament showed smooth surfaces with a thin, irregularly distributed powder layer (Fig. 11a–c, e, g), similar to nHA-coated PETG filament (Fig. 10a–c, e, g). A more obvious precipitation of nFA was visible in the area of the indentations by the gears (Fig. 11a arrow). Smallest nano-fluorapatite particles measured approximately 100 nm (Fig. 11g).

Using EDX analysis, carbon with a mass fraction of 44.79 %–52.31 % (Table 6) and oxygen of 30.55 %–31.75 % (Table 6) could be detected for PETG. An exception was filament sample C02, which composition was significantly lower for carbon, while the mass fractions of other elements were increased (Table 6). Detection of elements contained in nFA was possible in all three samples C01 – C03. Oxygen contained in nFA was not included, because its mass fractions were already assigned to PETG. The mass fraction of fluorine ranged from 1.27 % to 1.49 % (Table 6), for phosphorus from 1.35 % to 2.74 % (Table 6), and for calcium from 2.39 % to 5.38 % (Table 6). In PETG coated with nFA, sodium was also present in mass fractions of 0.16 %–0.54 % (Table 6).

In case of nano-fluorapatite coated PLA filament, it was not possible to acquire images exclusively using the SE detector due to charges, which is why a mixture of SE and BSE detectors was used. A powder layer made of nano-fluoropatite, which was irregular in distribution and thickness, was impressive. Deposits caused by irregularities from agglomerated nFA particles showed a size of up to approximately 15 μm for coated PLA (Fig. 11h*). Adding nFA powder followed by heat treatment smoothed out any unevenness in PLA, as it was previously the case with nHA. Smallest particles of nFA powder measured approximately 100 nm (Fig. 11h▲).

Mass fraction analysis of the surface composition revealed PLA values ranging from 18.41 % to 30.53 % for carbon (Table 6) and from 38.31 % to 45.35 % for oxygen (Table 6). An analysis of the components of nFA was also carried out, with detection of elements contained in nFA being possible in all three samples G01 - G03. Oxygen contained in nFA was not analyzed separately because it had already been assigned to PLA. Mass fractions of fluorine ranged from 0.78 % to 2.87 % (Table 6), for phosphorus from 1.67 % to 7.09 % (Table 6) and for calcium from 4.09 % to 14.45 % (Table 6). In addition, sodium could be detected in mass proportions of 0.35 %–0.87 % (Table 6). Except for the elements that are detectable from the coating process, such as gold and nitrogen, no other elements were contained in samples for PLA or PETG coated with nFA.

3.3. Determination of diameters of coated and uncoated filament

Diameters of coated and uncoated filaments were determined alternately at 90° angles using a micrometer screw gauge. Average values were obtained from 10 measurements (Table 7). The diameters resulted in average values of 1.748 mm for uncoated PETG and

Table 7
Diameter of coated and uncoated filaments in mm.

Filament	PETG	PLA	PETG + nHA	PLA + nHA	PETG + nFA	PLA + nFA
Measurement according to						
100 mm	1.751	1.752	1.767	1.759	1.760	1.756
200 mm	1.728	1.723	1.737	1.735	1.745	1.748
300 mm	1.749	1.773	1.771	1.759	1.760	1.757
400 mm	1.728	1.732	1.736	1.737	1.745	1.746
500 mm	1.769	1.769	1.767	1.768	1.758	1.756
600 mm	1.717	1.731	1.735	1.739	1.745	1.744
700 mm	1.761	1.762	1.758	1.763	1.757	1.755
800 mm	1.747	1.733	1.737	1.743	1.746	1.747
900 mm	1.784	1.772	1.761	1.767	1.759	1.757
1000 mm	1.749	1.736	1.737	1.739	1.749	1.749
Average	1.748	1.748	1.751	1.751	1.752	1.752
SD	0.019	0.018	0.015	0.013	0.007	0.005

The diameter of coated filaments was measured at a distance of 100 mm and recorded in mm. The measurement deviation of the micrometer screw gauge is 0.002 mm. SD indicates the standard deviation in mm, the mean is also given in mm.
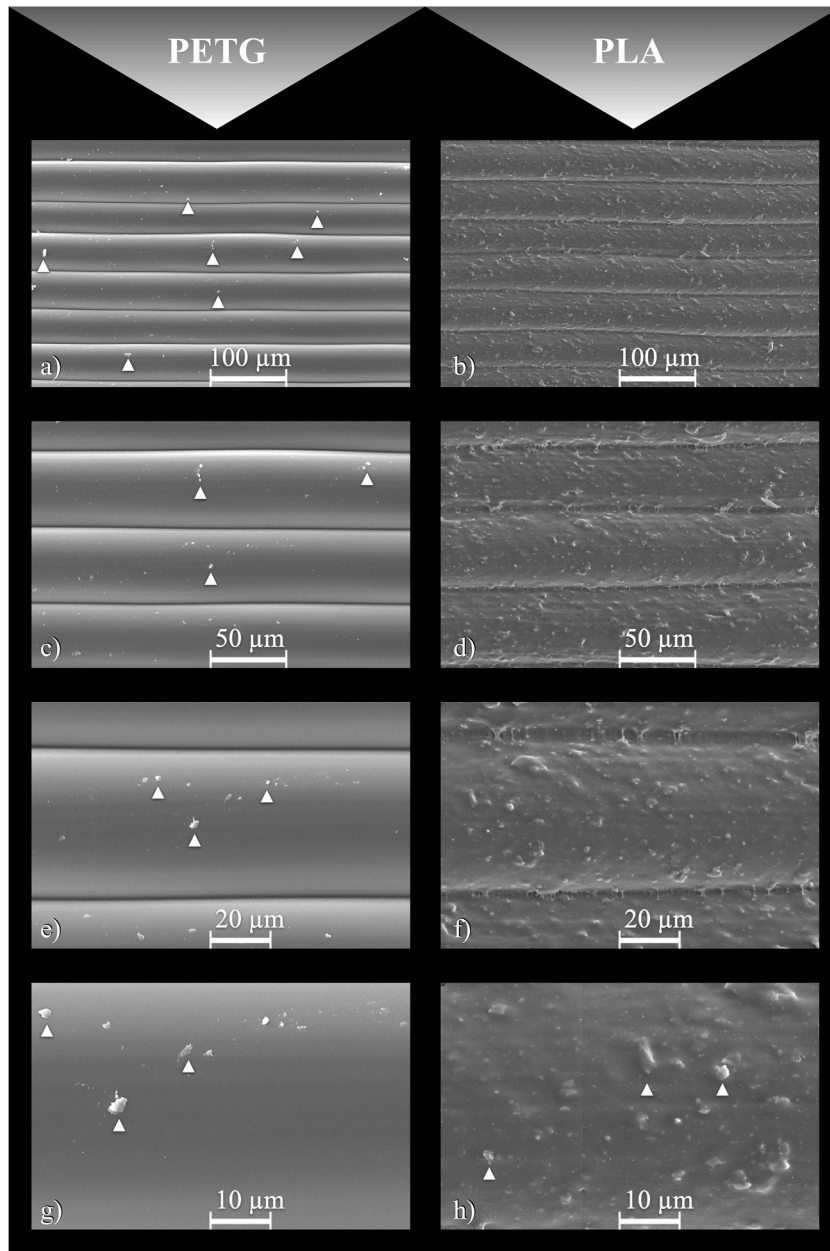
Fig. 12. SEM images of uncoated test specimens made of PETG and PLA filament
(a) test specimen made of PETG filament: magnification 250×
▲ indicate dust particles with sizes from 2 μm to 12.5 μm
(b) test specimen made of PLA filament: magnification 250×
(c) test specimen made of PETG filament: magnification 500×
▲ indicate dust particles with sizes from 2 μm to 12.5 μm
(dc) test specimen made of PLA filament: magnification 500×
(e) test specimen made of PETG filament: magnification 1,000×
▲ indicate dust particles with sizes from 1 μm to 3 μm
(f) test specimen made of PLA filament: magnification 1,000×
(g) test specimen made of PETG filament: magnification 2,000×
▲ indicate dust particles with sizes from 1 μm to 3 μm
(h) test specimen made of PLA filament: magnification 2,000×
▲ point to production-related particles with a size of 2–5 μm.

Table 8

Mass proportions of printed test specimens made of coated and uncoated filaments in wt%.

Sample	A05	A06	A07	E05	E06	E07	B05	B06	B07	F05	F06	F07	C05	C06	C07	G05	G06	G07
Elements	PETG	PETG	PETG	PLA	PLA	PLA	PETG + nHA	PETG + nHA	PETG + nHA	PLA + nHA	PLA + nHA	PLA + nHA	PETG + nFA	PETG + nFA	PETG + nFA	PLA + nFA	PLA + nFA	PLA + nFA
C	53.83	60.87	55.30	34.36	36.05	39.07	19.03	19.48	11.99	12.93	7.69	16.58	11.13	39.78	12.74	32.08	36.73	33.39
N	2.63	2.98	2.41	2.86	3.97	2.96	7.26	3.97	3.17	2.80	3.27	3.80	2.98	5.10	3.89	4.23	3.35	4.75
O	24.83	21.17	25.87	39.49	37.69	36.84	38.76	20.42	27.93	34.25	37.99	31.25	30.69	23.66	36.04	37.79	26.65	32.77
F								1.55	2.99				2.77	1.84	1.09	0.79	1.33	1.45
Na							1.60	0.39	0.59			0.68	0.64	0.74	0.17	0.52	0.59	0.57
P								9.92	12.21		10.90	9.02	10.48	3.69	9.53	0.40	1.52	1.65
Al							4.00											
Au	18.71	14.98	16.41	16.86	16.07	15.56	13.54	18.55	16.02	17.42	17.61	16.78	18.82	16.09	15.49	16.63	18.18	15.33
Cl							0.78											
K							2.19											
Ca				6.48	6.23	5.57	12.84	25.72	25.09	32.60	22.54	21.89	22.51	9.10	21.04	7.56	11.65	10.09

Note: Percentages represent mass fractions (Wt%). Values are rounded.

Abbreviations: Carbon (C), Nitrogen (N), Oxygen (O), Fluorine (F), Sodium (Na), Phosphorus (P), Aluminum (Al), Gold (Au), Chlorine (Cl), Potassium (K), Calcium (Ca).
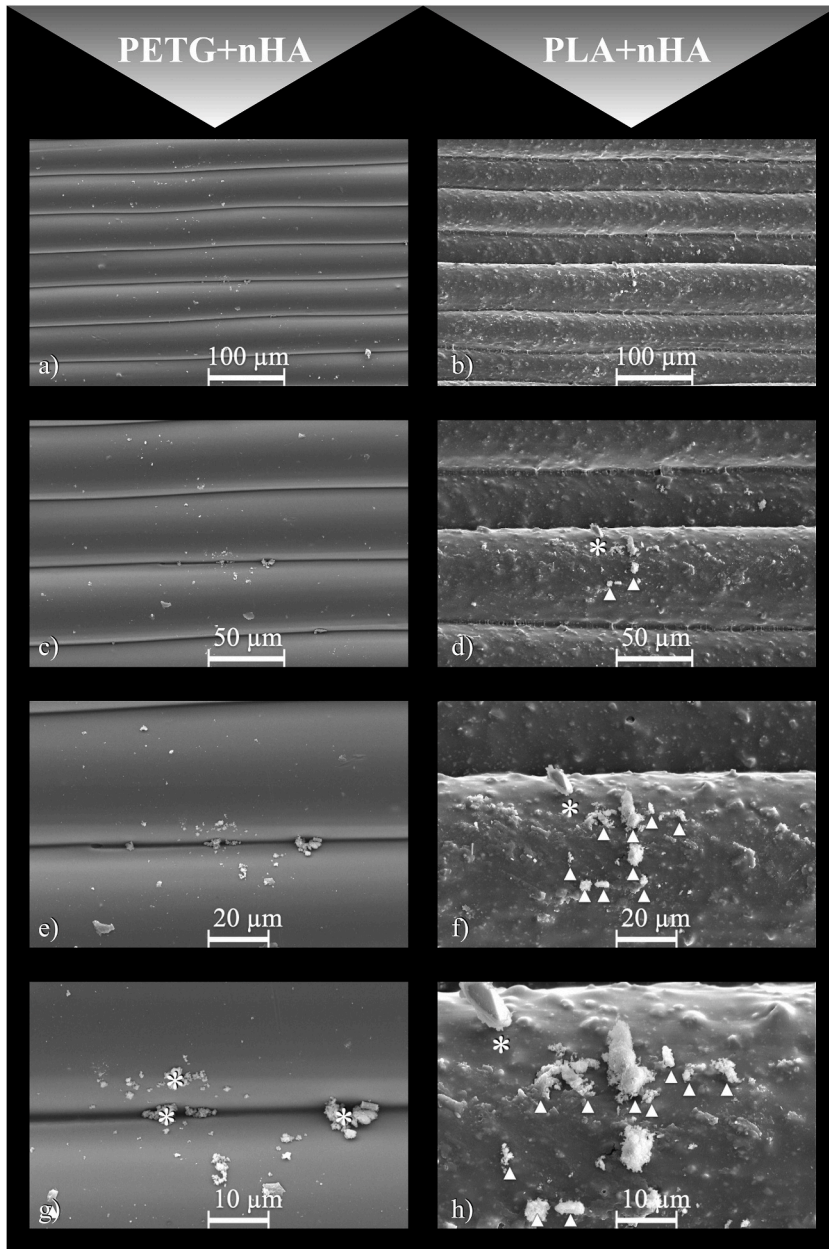
(caption on next page)

Fig. 13. SEM images of test specimens made of PETG coated with nHA
and PLA filament coated with nHA
(a) test specimen made of PETG filament coated with nHA: magnification 250×
(b) test specimen made of PLA filament coated with nHA: magnification 250×
(c) test specimen made of PETG filament coated with nHA: magnification 500×
(d) test specimen made of PLA filament coated with nHA: magnification 500×
▲ indicate incorporated nHA particles with sizes from 2 μm to 12.5 μm
* indicates partially incorporated nHA particles with a size of 10 μm
(e) test specimen made of PETG filament coated with nHA: magnification 1,000×
(f) test specimen made of PLA filament coated with nHA: magnification 1,000×
▲ indicate incorporated nHA particles with sizes from 2 μm to 12.5 μm
* indicates partially incorporated nHA particles with a size of 10 μm
(g) test specimen made of PETG filament coated with nHA: magnification 2,000×
▲ indicate incorporated nHA particles with sizes from 2 μm to 5 μm
* indicates partially incorporated nHA particles with a size of 10 μm
(h) test specimen made of PLA filament coated with nHA: magnification 2,000×
▲ indicate incorporated nHA particles with sizes from 2 μm to 12.5 μm
* indicates partially incorporated nHA particles with a size of 10 μm.

◀———

uncoated PLA. The diameters of coated filaments increased though: for PETG and PLA coated with nHA, an average diameter of 1.751 mm was measured. For PETG and PLA coated with nFA, the average diameter was 1.752 mm each. Coatings decreased standard deviation (SD) for all test series. Standard deviations were lowest for coatings with nFA, followed by coatings with nHA. However, the standard deviations were highest for uncoated filament.

3.4. Test specimen made of filament with and without coating

The cubic test specimens were first examined visually using magnifying glasses: no differences could be determined in all test specimens that were made from coated filament compared to test specimens made from uncoated filament. All showed a uniform, cubic shape without distortions. The side edges were congruent in shape without any excess. Surfaces of test specimens made of PLA filament, regardless of their coating, were perceived to be smoother than those made of PETG filament.

The surface morphology of side surfaces with and without folds, as well as the top surface, was then examined using SEM. In addition to a dense filling, all test specimens showed an even distribution of layers and a good connection between the layers.

Photographs of the PETG test specimens were taken at 250x to 2,000× magnification using a SE detector. Test specimens revealed smooth surfaces. Since sharp images in the area of the fold in test specimen A05 (Fig. 12a) were not possible even using BSE detector due to charging phenomena, the side surface was examined without the fold. There was a superficial deposit of dust particles ranging in size from 1 μm (Fig. 12g▲) to 12.5 μm (Fig. 12a▲) on side surfaces. When the samples were scanned through SEM, dust particles were removed, which meant that incorporation could be excluded.

EDX analysis determined mass fractions for carbon between 53.83 % and 60.87 % (Table 8) and for oxygen between 21.17 % and 25.87 % (Table 8).

SEM observation of test specimens made of PLA filament was also performed to examine the surface morphology of the printing results achieved. Using a SE detector, images with a magnification of 250× to 2,000x could be obtained, revealing a heterogeneous, rough surface with particles up to 5 μm in size (Fig. 12h). There was an analogy in the surface texture between individual layers of test specimens and PLA filament: particles were contained in both layers of the test specimens and in filament. As with test specimens made of PETG filament, sharp images were not possible in the area of the fold in test specimen E06 (Fig. 12b–d, f, h) due to charging phenomena, which is why a section of a side surface without a fold was chosen. For the subsequent examination of test specimens made of PETG and PLA filaments with coatings, the examination of side surfaces with folds was therefore omitted and a section of side surfaces without folds was chosen instead.

EDX analysis provided information about elements contained in test specimens made of PLA filament. Mass fractions for carbon ranged from 34.36 % to 39.07 % (Table 8) and for oxygen from 36.84 % to 39.49 % (Table 8). Using spot-on analysis, which was previously not possible with filament due to charging phenomena, ubiquitously occurring particles could be examined. This was caused by calcium responsible for the white color with mass proportions in PLA test specimens ranging from 5.57 % to 6.43 % (Table 8) Printed test specimens made of PETG and PLA also contained nitrogen and gold, which were created through the previously necessary coating process.

Photographs taken by SEM of test specimens made from PETG filament coated with nano-hydroxyapatite showed presence of deposition and partial incorporation of nHA-particles. Images were taken at 250x to 2,000× magnification using an SE detector. While test specimens made of pure PETG (Fig. 12a–c, e, g) had a smooth surface, all test specimens made from PETG filament coated with nHA showed rough surfaces due to absorbed nHA-particles with sizes of up to 10 μm (Fig. 13g*).

Since nHA was distributed randomly on the surface, an individual selection of the position and size of the analysis window for EDX was made for each test specimen, which, however, resulted in scattering of the values. First, mass fractions of the surface composition for PETG were examined: carbon made up a mass fraction of 11.99 %–19.48 % (Table 8) and oxygen made up a mass fraction of 20.42 %–38.76 % (Table 8). The reason for strong scatter in the mass fractions was size and position of the analysis windows, which were
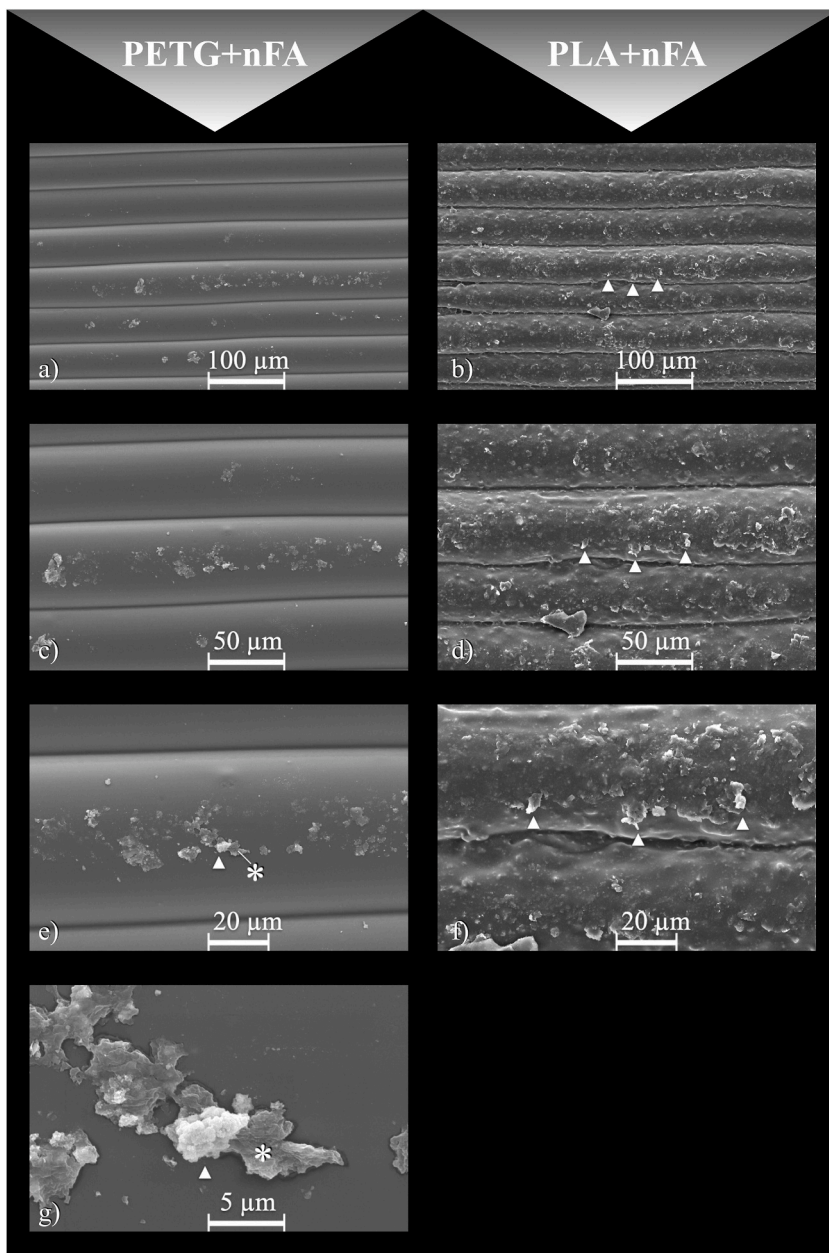
Fig. 14. SEM images of test specimens made of PETG coated with nFA
and PLA filament coated with nFA
(a) test specimen made of PETG filament coated with nFA: magnification 250×
(b) test specimen made of PLA filament coated with nFA: magnification 250×
▲ point to incorporated nFA particles with a size of 5 μm
c) test specimen made of PETG filament coated with nFA: magnification 500×
d) test specimen made of PLA filament coated with nFA: magnification 500×
▲ point to incorporated nFA particles with a size of
▲ show partially incorporated, agglomerated nFA particles with a size of 5 μm
* indicates a fully incorporated nFA particle with a size of 7.5 μm m
f) test specimen made of PLA filament coated with nFA: magnification 1,000×
▲ point to incorporated nFA particles with a size of 5 μm
g) test specimen made of PETG filament coated with nFA: magnification 2,000×
▲ show partially incorporated, agglomerated nFA particles with a size of 5 μm
* indicates a fully incorporated nFA particle with a size of 7.5 μm m.

selected based on visually visible powder precipitation. For components of nHA, calcium could be detected in all test specimens with mass fractions of 12.84 %–25.72 % (Table 8) and phosphorus of 9.92 % in test specimen B06 and 12.21 % (Table 8) in test specimen B07. In addition, other elements could be detected - although not in all test specimens - such as sodium with mass proportions of 0.39 %–1.60 % (Table 8), fluorine with 1.55 %–2.99 % (Table 8) and aluminum with 4.00 % (Table 8), chlorine with 0.78 % (Table 8) and potassium with 2.19 % (Table 8).

In test specimens made from PLA coated with nHA, there was additional build-up to the rough surface texture and sporadic incorporation of particles made of nHA. Nano-hydroxyapatite particles with sizes ranging from 2 μm to 12.5 μm (Fig. 13d–f, h▲) were found in layers. These particles could not be changed in position by the scanning process, but not all nano-hydroxyapatite particles were completely incorporated, like a particle approximately 10 μm in size (Fig. 13d–f, h*).

As with test specimens made of nHA-coated PETG, the distribution of nHA particles appeared isolated, requiring further individual adjustment of EDX analysis windows with limited comparability. When considering mass fractions of test specimens made from PLA coated with nHA, values for PLA for carbon ranged from 7.69 % (Table 8) to 16.58 % (Table 8) and for oxygen of 31.25 % (Table 8). to 37.99 % (Table 8). Calcium could be detected in mass fractions of 21.89 %–32.60 % (Table 8) and phosphorus contained in nHA from 9.02 % to 10.90 % (Table 8). Test specimen F07 also contained sodium with a mass fraction of 0.68 % (Table 8) below the detection limit. As with previous test specimens, gold and nitrogen (Table 8) were detectable by sputtering.

Images were taken using an SE detector at a magnification of 250 to 2000-fold of test specimens made from PETG filament coated with nano-fluoropatite powder. Test specimens showed rough surfaces due to agglomeration of nFA particles, some of which were embedded in pressure layers. The sizes of partially incorporated particles varied from 5 μm (Fig. 14e, g▲) to 7.5 μm (Fig. 14e, g*) with complete incorporation.

Due to sporadic distribution of nFA, the size and position of the analysis windows had to be adjusted individually for each sample, which limited comparison. Test specimens contained mass fractions of PETG with carbon from 11.13 % to 45.50 % (Table 8) and oxygen from 17.74 % to 36.04 % (Table 8). The surfaces were also examined for nano-fluorapatite, which contains calcium, phosphorus, oxygen and fluorine. Calcium was detectable in all three test specimens with mass fractions of 9.10 %–22.51 % (Table 8). Fluorine was also detectable in all three test specimens with mass fractions of 1.09 %–2.77 % (Table 8). In test specimen C05, phosphorus reached mass fractions of 3.69 %–10.48 % (Table 8), while sodium reached mass fractions of 0.17 %–0.74 % (Table 8).

SEM images of test specimens made of PLA filament with nFA coating were taken with an SE detector at a magnification level of 250 to 1000 times. Magnification levels beyond 1,000× were not possible due to strong charges. Print layers of test specimens made of PLA coated with nFA showed, like printed layers of test specimens made of PLA coated with nHA, additional deposits of calcium particles caused by production. A heterogeneous, rough surface of test specimens was evident in all test specimens which carrier material consisted of PLA, regardless of whether coated or uncoated PLA was used. Nano-fluorapatite particles with a size of up to 5 μm (Fig. 14b–d, f▲) were firmly incorporated into individual layers and could not be changed in position by scanning. However, here too, the distribution was sporadic, which made it necessary to adapt EDX analysis windows accordingly.

Carbon was represented with mass fractions of 32.08 %–36.73 % (Table 8) and oxygen with mass fractions of 26.65 %–37.79 % (Table 8). Calcium was present in mass fractions of 7.56 %–11.65 % (Table 8). Mass fractions of phosphorus and fluoride contained in nano-fluorapatite were also examined using EDX analysis. All elements were detectable. Fluorine was present at 0.79 %–1.45 % (Table 8) and phosphorus at 0.40 %–1.65 % (Table 8). Sodium was contained in all test specimens below the detection limit, with mass fractions between 0.52 % and 0.59 % (Table 8). Gold and nitrogen were detectable in PLA or PETG test specimens coated with nFA due to the necessary coating process.

4. Discussion

4.1. Composition of nanomaterials

As bioactive particles increase biocompatibility [11] this approach was implemented in the present work by using and adding biomimetic materials [82,83] in the form of nanomaterial [3] as hydroxylapatite and fluorapatite.

The EDX analysis of the nano-hydroxyapatite used showed mass fractions of oxygen of 30.76 %, of phosphorus of 12.16 % and of calcium of 23.89 %. Nano-fluorapatite was also subjected to EDX analysis. Mass fractions of oxygen were 32.22 %, of phosphorus 15.11 %, of calcium 32.48 % and of fluorine 3.58 %. In addition, sodium was present with a mass fraction of 0.98 %, which was within the detection limit. However, sodium is not a component of fluorapatite. Mass fractions of sodium could also be detected in nFA-coated PETG filaments at 0.16 %–0.35 % (Table 6) and in nFA-coated PLA filaments at 0.70 %–0.87 % (Table 6). For this reason, it is assumed that sodium was included during production. The addition of sodium during production raises the question of whether sodium fluoride (NaF) [84] was used. A calculation of the mass fractions of NaF results in 54.76 % for sodium and 45.24 % for fluorine. Mass fractions of sodium are present in a ratio of approximately 1.21 compared to fluorine. However, this ratio does not correspond to the EDX measurements for sodium, which were significantly lower than those for fluorine. For this reason, it is assumed that nFA did not contain NaF, but sodium was added for production reasons. The presence of sodium in further EDX analyzes was therefore considered as a component of nFA and not as an impurity when using nFA.

4.2. Composition of coated and uncoated filaments

PETG and PLA were used as carrier materials for the present experiments, because they are both biocompatible and classified as harmless by FDA [38,34]. Coated PETG could be used in further studies to produce crowns or splints, as it is an acid- and heat-resistant

material [34] and is already used in orthodontics for the production of splints [35]. PLA was used as further carrier material for filament in this work. Absorption and associated resorption of PLA in the human body [85] enables it to be used as a bone replacement material [30]. By adding nHA to PLA, an increase in bone volume is also possible [86].

Uncoated PETG filament showed a smooth surface texture (Fig. 9a–c). PLA, on the other hand, had a rough surface texture due to different levels of deposits on the filament of up to 40 μm (Fig. 9e). Since the coating machine did not supply heat for this series of tests, these deposits must have arisen during production of PLA filament. This manufacturing-related unevenness previously visible in the control group made of uncoated PLA filament appeared slightly leveled by heat treatment and addition of nHA. It measured approximately 15 μm in their greatest extent (Fig. 10h*). The added nano-hydroxyapatite powder apparently filled the unevenness present in the carrier material. There was also a leveling out of production-related unevenness in PLA when using nFA (Fig. 11h*).

The EDX analysis of PLA also provided information about the white color of the filament. In sample E05, an EDX spot-on analysis on the side surface of a cube-shaped test specimen proved an incorporated particle to consist of calcium, which had a mass fraction of 4.71 %–7.09 % (Table 6). The EDX analysis showed mass fractions for calcium of 9.80 %–18.95 % for PLA filament coated with nHA (Table 6). If mass proportions of calcium contained in uncoated PLA are subtracted from those in PLA coated with nHA, coatings result in an increase of 2.71 % in the minimum calculable concentration and in the maximum calculable concentration of 11.86 %. This means that additional calcium absorption and successful coating with nHA can be assumed. The same applies to coating with nFA. By using PLA filament with color particles in the present work, it can be demonstrated that it is possible to coat filament to which additives have already been added. Accordingly, recoating filaments already coated with nHA or nFA to increase the concentration would also be conceivable.

Nanoparticles of both the nHA and nFA-coated filaments were incorporated and could not be changed in position when scanned with the SEM. It can therefore be concluded that successful incorporation has taken place. The SEM images show a predominantly uniform distribution of the nHA or nFA particles. Overall, the distribution of nHA on PLA filament appeared significantly denser than of nHA on PETG filament. In EDX analysis, the proportion of nHA absorbed by PLA was higher than that of PETG. The same applied to the coating of nFA.

4.3. Contamination during the coating process

When PETG and PLA filaments were coated with nHA, all filament samples except sample B02, a PETG filament coated with nHA, were free of contamination of other elements. Sample B02 contained fluorine with a mass fraction of 1.04 % (Table 6) and sodium with a fraction of 0.41 % (Table 6). Since this only occurred with this sample, subsequent contamination during preparation or storage of the sample appeared possible.

Within the analytical capability of EDX, no additional elements were detectable in coated and uncoated filament. This would support a contamination-free passage through the coating device. However, it should be noted that contamination could be present in low concentrations that are not detectable using EDX analysis because they are below the detection limit.

4.4. Deviations in the diameter of coated and uncoated filament

Compared to filament extrudates produced using HME processes, deviations in diameter should be as small as possible [47,48,41, 42], which led to the development of the coating machine described. During the coating process, filament passes through a copper tube with an adjusted glass transition temperature of the respective filament of 100 °C for PETG [63] or 60 °C for PLA [67]. This should result in partial surface heating of filament, whereby particles of nHA or nFA are incorporated without changes in the filament diameter.

This was proven by a series of diameter measurements with a micrometer screw gauge, whereby measurement accuracy was ±2.0 μm. Uncoated PETG filament had a diameter of 1748 ± 0.019 mm and PLA filament 1748 ± 0.018 mm (Table 7). After coating with nHA, the diameter of PETG filament was 1751 ± 0.015 mm and of PLA filament was 1751 ± 0.013 mm (Table 7). When coated with nFA, the diameter of PETG filament was 1752 ± 0.007 mm and of PLA filament was 1752 ± 0.005 mm. The coating process reduced the standard deviation, resulting in a more uniform filament diameter.

The minor influence of the coating machine for filament on the filament diameter after coating was also demonstrated in the SEM. Impressions of the gears meshing during propulsion were visible on the surface of filaments in SEM images, regardless of whether it was uncoated control filament or whether it was heated filament coated with nanomaterials. The extent of the impressions was comparable: notches from gears were visible both in the control and coated filaments. If the glass transition temperature would have been exceeded, notches in the gears would have been less noticeable.

The limitation of this measuring method was the selection of a total 1000 mm long piece for each filament test series, which was then divided into ten 100 mm pieces each. This was due to the low availability of nHA and nFA limited the amount of harvested coated filament. An analysis of the diameters over the entire length of a respective filament test series would have led to a larger number of measurement results. The greater entity of these measurements might have compensated for production-related fluctuations in filament diameter before the coating process.

4.5. Composition of coated and uncoated test specimens

When viewed using SEM, dust particles were visible on the side surfaces of test specimens from the control group made of PETG filament, which could be removed by scanning. Electrostatic charging phenomena on smooth side surfaces are suspected to be the

reason of dust accumulation. EDX analysis showed only a slight difference in mass proportions between PETG filament and test specimens made from PETG filament.

Dust particles that occurred on smooth surfaces in test specimens made from PETG filament were not detectable in test specimens in the control group made from PLA. However, test specimens made of PLA had rough surfaces due to the presence of calcium particles. These rough surfaces of PLA test specimens remain even when coated with nHA or nFA.

The distribution of nHA or nFA in test specimens made of filament coated filament was lower than for the corresponding coated filaments when viewed using SEM (see Fig. 10 compared to Figs. 13 and 11 compared to Fig. 14). This could be due to the fact that the coated filament is mixed in the extruder. The powder coating on the surface of the filament seems to be distributed during the extrusion process while printing. This leads to a lower number of nanoparticles on the printed surface compared to the surface of the coated filament. By SEM detecting of nHA and nFA on the surface of printed test specimens, it was also possible to show that nHA and nFA adhere to the surface of the filament during the coating process in such a way that they are also processed in the printing process. They are incorporated in the filament while extrusion printing.

In the EDX analysis of test specimens made from nHA-coated PETG, only a limited comparison was possible due to varying position and size of analysis windows. No phosphorus was detectable in test specimen B05, possibly due to an unsuitable selection of the analysis window.

Phosphorus was present in test specimens printed from nHA-coated PLA with mass fractions of 9.02 %–10.90 % (Table 8). In all three test specimens, which were made from PLA coated with nHA, calcium mass fractions of 21.89 %–32.60 % (Table 8) were detected, which significantly exceeded the values of the control group. If differences are formed between mass fractions of calcium from test specimens made with nHA-coated PLA (Table 8) and mass fractions of calcium from test specimens (Table 6) made of PLA without additives, an excess due to the coating of nHA can be calculated. This ranges from 15.46 % to 27.03 %. An excess of calcium was also found in test specimens made of PLA coated with nFA. However, the surplus here was lower at 1.08 %–6.08 %.

Completely incorporated particles varied in size of 5–20 μm regardless of the filament and nanomaterial used. Mass fractions of test specimens consisting of nHA-coated filament appeared to be lower when visually observed by SEM than those of test specimens consisting of nFA-coated filament. Compared to nFA-coated PETG, mass fractions of PLA coated with nFA appeared to be lower, although different analysis windows may be the reason for this. Overall, the analysis windows had to be chosen according to the sporadic occurrence of nanoparticles, which limits direct comparison.

4.6. Abrasion and contamination after printing using coated and uncoated filament

For test specimens made of pure PETG and PLA filament, no other elements were detectable in the EDX analysis. It can therefore be assumed that there was no material abrasion or contamination during the printing process with PETG and PLA filaments.

In test specimens made from filament coated with nHA, additional elements were found, especially in PETG, which could not be explained by the addition of hydroxyapatite: sodium was present in mass proportions of 0.39 %–1.60 % (Table 8). In addition, fluorine was detectable at 1.55 % (Table 8) in test specimen B06 and at 2.99 % in B07 (Table 8). The presence of fluorine could also not be reconciled with the composition of nHA. PETG filament was the first filament in the test series to be coated with nHA. PLA filament was then coated with nHA and only then were series of tests with nFA coatings followed. Given the chronology of the coating processes, contamination in the coating device is out of the question. Instead, contamination may have occurred due to storage of nHA-coated PETG filament in a 3l general-purpose bag.

Subsequent contamination also occurred in test specimen F07, which was made from PLA coated with nHA and contained sodium with a mass fraction of 0.68 % (Table 8). The rest of the test series had no other elements.

In one test specimen made out of PETG and nHA (B05, Table 8), mass fractions of aluminum were also detected at 4.00 %, chlorine at 0.78 % and potassium at 2.19 %. Since particles of these various elements were already incorporated into test specimen B05, there could not have been any subsequent contamination of the test specimen with aluminum, chlorine and potassium. The presence of these elements in test specimen B05 may have resulted from abrasion in the hotend. In this, filament is melted and then distributed onto the print sheet by the printer nozzle. Abrasive materials can release particles from the alloy in the hotend, which then later fuse with filament in the print. This appeared to be the case with sample B05 using nHA.

4.7. Limitations of SEM imaging and analysis

To examine mass fractions contained, analysis windows had to be individually adjusted when looking at printed test specimens, as incorporated particles of nHA or nFA were sporadically and not ubiquitously distributed. This means that comparability, particularly of the test specimens in terms of mass proportions, is only possible to a limited extent. Due to sporadic distribution of nanoparticles, no other approach could be chosen as the experimental procedure should maintained.

In order to be able to make a statement about the actual coating of nHA and nFA, cross-sections of coated and uncoated filaments were examined using SEM and EDX in preliminary tests. However, both PETG and PLA filaments proved to be too ductile when cut with scalpels, meaning that straight, unadulterated cross-sections could not be harvested. In addition, the cross sections were crooked, meaning that this method could not be used for further evaluations. Other different methods were used to obtain cross sections: Cross sections of polymer membranes can be obtained conventionally by means of fracture after an immersion bath in liquid nitrogen for 5 min [87]. However, this process, also known as direct freeze fracture [88] could not be implemented with polymer filaments, nor could a modified variant known as "cryo-snap" [88] because brittle fracture with a straight cut surface did not occur. Bead-like deformations in the cutting area led to charging artifacts that made analysis with EDX impossible.

Table 9
Particle concentration of coated and uncoated filament in ppm.

filament	average diameter (d) in mm	Cross-sectional area (A) $= \pi \times (d/2)^2$	added particles in ppm $= ((A_{coated\ filament}/A_{control\ group}) - 1) \times 10^6$
control group			
PETG	1.748	2.400	0
PLA	1.748	2.400	0
coated filament with nHA			
PETG + nHA	1.751	2.408	3.435
PLA + nHA	1.751	2.408	3.435
coated filament with nFA			
PETG + nFA	1.752	2.411	4.582
PLA + nFA	1.752	2.411	4.582

4.8. Suitability and limitation of the coating machine for filament

The procedures described for the production process of filaments with additives, such as impregnation processes, are ruled out due to their time-consuming implementation [54,55]. Other methods are unsuitable due to limited material selection [56,89,90] or time-consuming processing [52,53,50,51]. The HME process is also worth mentioning as an admixture for thermoplastics, as it is already used in pharmaceutical production [1] and experimentally in dentistry [47,48]. However, filament extrudates produced using the HME process exhibit deviations in terms of diameter [47,48,41,42]. As a result, the use of these filaments might result in over- or undershoots in individual filament layers. For dentistry a nozzle with a diameter of 0.25 mm is required due to higher-resolution extrusion prints. This increases over- and undershoots of extruded filament by 60 % compared to printing with a nozzle with a diameter of 0.40 mm. For this reason, the filament diameter should be as constant as possible, which led to the proposed coating machine for filament. During the coating process, the filament passes through a copper tube whose temperature corresponds to the glass transition temperature of the respective filament of 100 °C for colorFabb_HT clear [63] or 60 °C for extrudr PLA NX2 white [67]. This should result in partial surface heating of the filament, whereby particles of nHA or nFA are incorporated without changes in the filament diameter occurring. Possible unevenness of the filament, which manifests itself in a deviation of the diameter, could be compensated by the passage of the copper tube. This could be verified by measuring the diameter with measuring spindle of a micrometer with a measuring accuracy of ±2.0 μm.

An approximate indication of the percentage admixture by coating is possible by dividing the average cross-sectional area of coated filaments by the cross-sectional area of uncoated filaments. This does not take into account the change in shape of the cross-section caused by the plateau-like leveling due to the indentations, which is why the results (Table 9) should be regarded as estimates. PETG or PLA filament coated with nHA would therefore have a particle concentration of approximately 3400 ppm, while the concentration of PETG or PLA filament coated with nFA would be approximately 4600 ppm. Filament coated nano-fluorapatite exceeds the fluoride concentrations of 1500 ppm in conventionally available toothpastes and reaches a concentration of approximately 5000 ppm, as found in therapeutically prescribed toothpastes [84]. This means that filament coated with nFA could be used to produce caries-preventive dental products such as splints.

The coating machine was used to produce small quantities for the individual needs of patients. The average filament throughput was 410 mm per minute after the glass transition temperature of the filament was reached after 5 min of operating time. Assuming an average filament diameter of 1.751 mm for coating with nHA, this results in a volume per minute of:

$$V_{filament} = \pi \times r_{filament}^2 \times h_{filament} \text{ with } r_{filament} = 0.8755 \text{ mm}$$

with $h_{filament} = 410 \text{ mm}$

$V_{filament} = 987{,}29 \text{ mm}^3$

$= 0.98729 \text{ cm}^3$

For PETG (colorFabb_HT clear), the density is 1.2 g/cm^3 [63], while PLA (extrudr PLA NX2 white) has a higher density of 1.3 g/cm^3 [67]. The mass that is coated within 1 min can therefore be calculated as follows:

$$m_{filament} = \rho_{filament} \times V_{filament}$$

$$m_{PETG} = \rho_{PETG} \times V_{filament} \text{ with } \rho_{PETG} = 1.2 \text{ g / cm}^3$$

$$= 1.2 \text{ g / cm}^3 \times 0.98729 \text{ cm}^3$$

$$= 1.1848 \text{ g}$$

$$m_{PLA} = \rho_{PLA} \times V_{filament} \text{ with } \rho_{PLA} = 1.3 \text{ g / cm}^3$$

$$= 1.3 \text{ g / }_{cm3} \times 0.98729 \text{ cm}^3$$

=1.2835 g

Calculating the volume for filament coated with nFA results in a volume of 988,42 mm^3 or 0.98842 cm^3 per minute. This results in a mass of 1.1861 g for coating of PETG with nFA and 1.2849 g for coating of PLA with nFA within a minute. Approximately 1.2 g of PETG (colorFabb_HT clear) and 1.3 g of PLA (extrudr PLA NX2 white) can be processed per minute with the coating machine for filament. In this way, it is possible to produce small quantities of patient-specific quantities, making it possible to implement personalized medicine [3,4,2] in the field of dentistry.

5. Conclusion

This proof of concept study aims to investigate whether a process can be developed to produce filament-based, biomimetic and bioactive 3D printing materials for medicine and dentistry. This has been proven by successfully coating PETG or PLA filament with nHA or nFA. The advantages of the coating machine for filament lie in the fact that.

(i) The coating process reduced the standard deviation of filament diameter. Deviations in the filament diameter could be leveled out, while at the same time thickness of filament increased slightly due to coating. This resulted in a more uniform filament diameter. A more uniform diameter improves printing quality of extrusion printing.

(ii) A production of coated filament in small quantities in the reach of grams can be achieved with the coating machine for filament. This enables the implementation of personalized medicine in various specialist disciplines, which, in addition to the development of restorative materials in dentistry, also enables the development of bio- or bone replacement materials in medicine. As tensile properties of polymers are improved by the addition of nanoparticles [91], the usage of the coating machine offers further potential not only in dentistry and medicine. The coating machine for filament also enables the realization of an economical and resource-friendly production of small amounts for testing and experimental approaches of new coatings.

(iii) The coating of filament can be carried out with the proposed coating machine for filament.Coated filament was also suitable for producing test specimens, with no differences in the printing results with uncoated filament. In addition to PETG and PLA, the coating of other thermoplastic polymers is also conceivable. For other polymers, the heating temperature of the peltier elements must be adjusted according to the glass transition temperature. For example, polyamide could be coated, whereby the peltier elements would have to reach a temperature of 70 °C, this would be the case with a current of 3.5 A (see Table 1).

(iv) The print quality of coated filaments showed comparable results compared to that of uncoated filaments. No difference between the specimen made of coated and uncoated filament could be detected in the SEM examination.

(v) Coating filament takes approximately 30 min, depending on the desired quantity. This makes it possible to use individualized filament tailored to the patient's needs for MEX printing as a chairside application in the dental practice. Furthermore the coating machine for filament could enable a rapid extrusion prototyp production with the use of coated filament for technical applications.

All the points listed in the COI were successfully implemented with the coating machine for filament, thus providing proof of concept.

CRediT authorship contribution statement

Ulf Tilman Strähle: Writing – original draft, Visualization, Validation, Resources, Project administration, Methodology, Investigation, Data curation, Conceptualization. **Norbert Pütz:** Visualization, Investigation, Data curation. **Matthias Hannig:** Writing – review & editing, Validation, Supervision, Project administration, Conceptualization.

Declaration of competing interest

The authors declare that they have no known competing financial interests or personal relationships that could have appeared to influence the work reported in this paper.

References

[1] Alruwaili NK. Ameeduzzafar, M. Rizwanullah, S.N. Abbas Bukhari, M. Amir, M.M. Ahmed, M. Fazil, D Printing Technology in Design of Pharmaceutical Products, Curr Pharm Des 24 (42) (2018) 5009–5018, https://doi.org/10.2174/1381612825666190116104620.

[2] N. Sandler, M. Preis, Printed drug-delivery systems for improved patient treatment, Trends Pharmacol. Sci. 37 (12) (2016) 1070–1080, https://doi.org/10.1016/j.tips.2016.10.002.

[3] M. Di Sanzo, L. Cipolloni, M. Borro, R. La Russa, A. Santurro, M. Scopetti, et al., Clinical applications of personalized medicine: a new paradigm and challenge, Curr Pharm Biotechnol 18 (3) (2017) 194–203, https://doi.org/10.2174/1389201018666170224105600.

[4] D. Ho, S.R. Quake, E.R.B. McCabe, W.J. Chng, E.K. Chow, X. Ding, et al., Enabling technologies for personalized and precision medicine, Trends Biotechnol. 38 (5) (2020) 497–518, https://doi.org/10.1016/j.tibtech.2019.12.021.

[5] N. Dumpa, A. Butreddy, H. Wang, N. Komanduri, S. Bandari, M.A. Repka, 3D printing in personalized drug delivery: an overview of hot-melt extrusion-based fused deposition modeling, Int J Pharm 600 (2021) 120501, https://doi.org/10.1016/j.ijpharm.2021.120501.

[6] X. Xu, A. Awad, P. Robles-Martinez, S. Gaisford, A. Goyanes, A.W. Basit, Vat photopolymerization 3D printing for advanced drug delivery and medical device applications, J Control Release 329 (2021) 743–757, https://doi.org/10.1016/j.jconrel.2020.10.008.

[7] B.C. Gross, J.L. Erkal, S.Y. Lockwood, C. Chen, D.M. Spence, Evaluation of 3D printing and its potential impact on biotechnology and the chemical sciences, Anal. Chem. 86 (7) (2014) 3240–3253, https://doi.org/10.1021/ac403397r.

[8] M. Livesu, S. Ellero, J. Martínez, S. Lefebvre, M. Attene, From 3D models to 3D prints: an overview of the processing pipeline, Comput. Graph. Forum 36 (2) (2017) 537–564, https://doi.org/10.1111/cgf.13147.

[9] S. Deshkar, M. Rathi, S. Zambad, K. Gandhi, Hot melt extrusion and its application in 3D printing of pharmaceuticals, Curr. Drug Deliv. 18 (4) (2021) 387–407, https://doi.org/10.2174/1567201817999201110193655.

[10] C.C. Coelho, L. Grenho, P.S. Gomes, P.A. Quadros, M.H. Fernandes, Nano-hydroxyapatite in oral care cosmetics: characterization and cytotoxicity assessment, Sci. Rep. 9 (1) (2019) 11050, https://doi.org/10.1038/s41598-019-47491-z.

[11] K. Pajor, L. Pajchel, J. Kolmas, Hydroxyapatite and fluorapatite in conservative dentistry and oral implantology-A review, Materials 12 (17) (2019), https://doi.org/10.3390/ma12172683.

[12] L. Wang, X. Guan, H. Yin, J. Moradian-Oldak, G.H. Nancollas, Mimicking the self-organized microstructure of tooth enamel, J Phys Chem C Nanomater Interfaces 112 (15) (2008) 5892–5899.

[13] L. Chen, S. Al-Bayatee, Z. Khurshid, A. Shavandi, P. Brunton, J. Ratnayake, Hydroxyapatite in oral care products-A review, Materials 14 (17) (2021).

[14] W.D. Browning, S.D. Cho, E.J. Deshepper, Effect of a nano-hydroxyapatite paste on bleaching-related tooth sensitivity, J. Esthetic Restor. Dent. 24 (4) (2012) 268–276, https://doi.org/10.1111/j.1708-8240.2011.00437.x.

[15] S. Huang, S. Gao, L. Cheng, H. Yu, Remineralization potential of nano-hydroxyapatite on initial enamel lesions: an in vitro study, Caries Res. 45 (5) (2011) 460–468, https://doi.org/10.1159/000331207.

[16] M. Hannig, C. Hannig, Nanotechnology and its role in caries therapy, Adv. Dent. Res. 24 (2) (2012) 53–57, https://doi.org/10.1177/0022034512450446.

[17] R.J. Wierichs, T.G. Wolf, G. Campus, T.S. Carvalho, Efficacy of nano-hydroxyapatite on caries prevention—a systematic review and meta-analysis, Clin. Oral Invest. 26 (4) (2022) 3373–3381.

[18] F.H. Albee, Studies in bone growth: Triple calcium phosphate as a stimulus to osteogenesis, Ann. Surg. 71 (1) (1920) 32–39, https://doi.org/10.1097/00000658-192001000-00006.

[19] S. Wei, J.-X. Ma, L. Xu, X.-S. Gu, X.-L. Ma, Biodegradable materials for bone defect repair, Military Medical Research 7 (1) (2020) 54, https://doi.org/10.1186/s40779-020-00280-6.

[20] M. Yazdanian, A. Rahmani, E. Tahmasebi, H. Tebyanian, A. Yazdanian, S.A. Mosaddad, Current and advanced nanomaterials in dentistry as regeneration agents: an update, Mini Rev. Med. Chem. 21 (7) (2021) 899–918, https://doi.org/10.2174/1389557520666201124143449.

[21] I.R. Bordea, S. Candrea, G.T. Alexescu, S. Bran, M. Băciuţ, G. Băciuţ, et al., Nano-hydroxyapatite use in dentistry: a systematic review, Drug Metabol. Rev. 52 (2) (2020) 319–332, https://doi.org/10.1080/03602532.2020.1758713.

[22] M. Özcan, D. Hotza, M.C. Fredel, A. Cruz, C.A.M. Volpato, Materials and manufacturing techniques for polymeric and ceramic scaffolds used in implant dentistry, Journal of Composites Science 5 (3) (2021) 78, https://doi.org/10.3390/jcs5030078.

[23] C.M.G. Nobre, N. Putz, M. Hannig, Adhesion of hydroxyapatite nanoparticles to dental materials under oral conditions, Scanning 2020 (2020) 6065739, https://doi.org/10.1155/2020/6065739.

[24] N. Leroy, E. Bres, Structure and substitutions in fluorapatite, Eur. Cell. Mater. 2 (2001) 36–48, https://doi.org/10.22203/ecm.v002a05.

[25] N. Montazeri, R. Jahandideh, E. Biazar, Synthesis of fluorapatite-hydroxyapatite nanoparticles and toxicity investigations, Int J Nanomedicine 6 (2011) 197–201, https://doi.org/10.2147/ijn.s15461.

[26] C.J. Mc, W.C. Foster, Prevention of dental caries by brushing the teeth with powders containing fluorapatite, J. Dent. Res. 26 (3) (1947) 233–239, https://doi.org/10.1177/00220345470260030601406.

[27] R. Palanivelu, S. Sundharam, K. Sivasubramanian, Nano-characterization and in vitro bioactivity of chemically synthesized fluorapatite, Journal of the Australian Ceramic Society 58 (5) (2022) 1603–1614, https://doi.org/10.1007/s41779-022-00797-0.

[28] Y. Moayedee, I. Mobasherpour, S. Banijamali, M. Razavi, N. Nezafati, Effect of the nano-fluorapatite ceramic particles on mechanical behavior of fluoride varnishes, Mater. Chem. Phys. 288 (2022) 126421, https://doi.org/10.1016/j.matchemphys.2022.126421.

[29] D.F. Williams, On the mechanisms of biocompatibility, Biomaterials 29 (20) (2008) 2941–2953, https://doi.org/10.1016/j.biomaterials.2008.04.023.

[30] R.K. Kulkarni, E.G. Moore, A.F. Hegyeli, F. Leonard, Biodegradable poly(lactic acid) polymers, J. Biomed. Mater. Res. 5 (3) (1971) 169–181, https://doi.org/10.1002/jbm.820050305.

[31] Z. Terzopoulou, A. Zamboulis, I. Koumentakou, G. Michailidou, M.J. Noordam, D.N. Bikiaris, Biocompatible synthetic polymers for tissue engineering purposes, Biomacromolecules 23 (5) (2022) 1841–1863, https://doi.org/10.1021/acs.biomac.2c00047.

[32] V. DeStefano, S. Khan, A. Tabada, Applications of PLA in modern medicine, Engineered Regeneration 1 (2020) 76–87, https://doi.org/10.1016/j.engreg.2020.08.002.

[33] T. Serra, M.A. Mateos-Timoneda, J.A. Planell, M. Navarro, 3D printed PLA-based scaffolds, Organogenesis 9 (4) (2013) 239–244, https://doi.org/10.4161/org.26048.

[34] S. Petersmann, M. Spoerk, W. Van De Steene, M. Üçal, J. Wiener, G. Pinter, F. Arbeiter, Mechanical properties of polymeric implant materials produced by extrusion-based additive manufacturing, J. Mech. Behav. Biomed. Mater. 104 (2020) 103611, https://doi.org/10.1016/j.jmbbm.2019.103611.

[35] L. Šimunović, T. Blagec, S. Meštrović, Resistance of PETG materials on thermocycling and brushing, Dent. J. 11 (5) (2023) 135, https://doi.org/10.3390/dj11050135.

[36] T. Balint, J. Živčák, R. Hudák, T. Tóth, M. Kohan, S. Lancoš, Destructive and non-destructive testing of samples from PLA and PETG materials, IOP Conf. Ser. Mater. Sci. Eng. 1199 (1) (2021) 012045, https://doi.org/10.1088/1757-899X/1199/1/012045.

[37] M.H. Hassan, A.M. Omar, E. Daskalakis, Y. Hou, B. Huang, I. Strashnov, et al., The potential of polyethylene terephthalate glycol as biomaterial for bone tissue engineering, Polymers 12 (12) (2020), https://doi.org/10.3390/polym12123045.

[38] S. Farah, D.G. Anderson, R. Langer, Physical and mechanical properties of PLA, and their functions in widespread applications — a comprehensive review, Adv. Drug Deliv. Rev. 107 (2016) 367–392, https://doi.org/10.1016/j.addr.2016.06.012.

[39] K. Wakamori, K. Nagata, T. Nakashizu, H. Tsuruoka, M. Atsumi, H. Kawana, Comparative verification of the accuracy of implant models made of PLA, resin, and silicone, Materials 16 (9) (2023) 3307, https://doi.org/10.3390/ma16093307.

[40] H. Patil, R.V. Tiwari, M.A. Repka, Hot-melt extrusion: from theory to application in pharmaceutical formulation, AAPS PharmSciTech 17 (1) (2016) 20–42.

[41] H. Ponsar, R. Wiedey, J. Quodbach, Hot-melt extrusion process fluctuations and their impact on critical quality attributes of filaments and 3D-printed dosage forms, Pharmaceutics 12 (6) (2020), https://doi.org/10.3390/pharmaceutics12060511.

[42] J.A. Weisman, J.C. Nicholson, K. Tappa, U. Jammalamadaka, C.G. Wilson, D.K. Mills, Antibiotic and chemotherapeutic enhanced three-dimensional printer filaments and constructs for biomedical applications, Int J Nanomedicine 10 (2015) 357–370, https://doi.org/10.2147/ijn.s74811.

[43] E. Mathew, J. Dominguez-Robles, S.A. Stewart, E. Mancuso, K. O'Donnell, E. Larraneta, D.A. Lamprou, Fused deposition modeling as an effective tool for anti-infective dialysis catheter fabrication, ACS Biomater. Sci. Eng. 5 (11) (2019) 6300–6310, https://doi.org/10.1021/acsbiomaterials.9b01185.

[44] C. Liu, Z. Xia, J.T. Czernuszka, Design and development of three-dimensional scaffolds for tissue engineering, Chem. Eng. Res. Des. 85 (7) (2007) 1051–1064, https://doi.org/10.1205/cherd06196.

[45] W. Wang, B. Zhang, L. Zhao, M. Li, Y. Han, L. Wang, et al., Fabrication and properties of PLA/nano- HA composite scaffolds with balanced mechanical properties and biological functions for bone tissue engineering application, Nanotechnol. Rev. 10 (1) (2021) 1359–1373, https://doi.org/10.1515/ntrev-2021-0083.

[46] W. Wang, B. Zhang, M. Li, J. Li, C. Zhang, Y. Han, et al., 3D printing of PLA/n-HA composite scaffolds with customized mechanical and biological functions for bone tissue engineering, Compos. B Eng. 224 (2021) 109192, https://doi.org/10.1016/j.compositesb.2021.109192.

[47] V. Berger, Z. Luo, J.-C. Leroux, 3D printing of a controlled fluoride delivery device for the prevention and treatment of tooth decay, J. Contr. Release 348 (2022) 870–880, https://doi.org/10.1016/j.jconrel.2022.06.032.

[48] K. Liang, S. Carmone, D. Brambilla, J.-C. Leroux, 3D printing of a wearable personalized oral delivery device: a first-in-human study, Sci. Adv. 4 (5) (2018) eaat2544, https://doi.org/10.1126/sciadv.aat2544.

[49] 3D model preparing for rapid prototyping by FDM method, in: K. Dvorak (Ed.), 2017 8th International Conference on Mechanical and Aerospace Engineering, ICMAE, 2017 , https://doi.org/10.1109/ICMAE.2017.8038611.

[50] N. Vidakis, A. Moutsopoulou, M. Petousis, N. Michailidis, C. Charou, N. Mountakis, et al., Medical- grade PLA nanocomposites with optimized tungsten carbide nanofiller content in MEX additive manufacturing: a rheological, morphological, and thermomechanical evaluation, Polymers 15 (19) (2023) 3883, https://doi.org/10.3390/polym15193883.

[51] N. Vidakis, M. Petousis, E. Velidakis, M. Liebscher, L. Tzounis, Three-Dimensional printed antimicrobial objects of polylactic acid (PLA)-Silver nanoparticle nanocomposite filaments produced by an in-situ reduction reactive melt mixing process, Biomimetics 5 (3) (2020) 42, https://doi.org/10.3390/biomimetics5030042.

[52] M. Petousis, N. Michailidis, V. Saltas, V. Papadakis, M. Spiridaki, N. Mountakis, et al., Mechanical and electrical properties of polyethylene terephthalate glycol/antimony tin oxide nanocomposites in material extrusion 3D printing, Nanomaterials 14 (9) (2024) 761, https://doi.org/10.3390/nano14090761.

[53] M. Petousis, N. Vidakis, N. Mountakis, V. Papadakis, S. Kanellopoulou, A. Gaganatsiou, et al., Multifunctional material extrusion 3D-printed antibacterial polylactic acid (PLA) with binary inclusions: the effect of cuprous oxide and cellulose nanofibers, Fibers 10 (6) (2022) 52, https://doi.org/10.3390/fib10060052.

[54] S. Bandari, D. Nyavanandi, N. Dumpa, M.A. Repka, Coupling hot melt extrusion and fused deposition modeling: critical properties for successful performance, Adv. Drug Deliv. Rev. 172 (2021) 52–63, https://doi.org/10.1016/j.addr.2021.02.006.

[55] K.-M. Lee, H. Park, J. Kim, D.-M. Chun, Fabrication of a superhydrophobic surface using a fused deposition modeling (FDM) 3D printer with poly lactic acid (PLA) filament and dip coating with silica nanoparticles, Appl. Surf. Sci. 467–468 (2019) 979–991, https://doi.org/10.1016/j.apsusc.2018.10.205.

[56] P. Chohan, A. Yadav, R. Kumar, R. Kumar, S.J. Chohan, An apparatus designed for coating and coloration of filaments used in fused filament fabrication (FFF) 3D printing, Recent Pat. Mech. Eng. 14 (4) (2021) 541–549, https://doi.org/10.2174/2212797614666210208224615.

[57] C.M. Cheah, C.K. Chua, C.W. Lee, C. Feng, K. Totong, Rapid prototyping and tooling techniques: a review of applications for rapid investment casting, Int. J. Adv. Des. Manuf. Technol. 25 (3–4) (2004) 308–320, https://doi.org/10.1007/s00170-003-1840-6.

[58] K.K. Jurrens, Standards for the rapid prototyping industry, Rapid Prototyp. J. 5 (4) (1999) 169–178, https://doi.org/10.1108/13552549910295514.

[59] Y. Yan, S. Li, R. Zhang, F. Lin, R. Wu, Q. Lu, et al., Rapid prototyping and manufacturing technology:principle, representative technics, applications, and development trends, Tsinghua Sci. Technol. 14 (2009) 1–12, https://doi.org/10.1016/S1007-0214(09)70059-8.

[60] T.S. Jones, R.C. Richey, Rapid prototyping methodology in action: a developmental study, Educ. Technol. Res. Dev. 48 (2) (2000) 63–80, https://doi.org/10.1007/BF02313401.

[61] J.C. Goldsack, A.V. Dowling, D. Samuelson, B. Patrick-Lake, I. Clay, Evaluation, acceptance, and qualification of digital measures: from proof of concept to endpoint, Digit. Biomark. 5 (1) (2021) 53–64, https://doi.org/10.1159/000514730.

[62] Information of colorFabb_HT Clear, URL retrieved on 2024.05.21: https://colorfabb.com/de/ht-clear.

[63] Technical Data Sheet of colorFabb_HT Clear, URL retrieved on 2024.05.16: https://downloads.colorfabb.com/index.php/s/rtfDDRCa723Xdor?path=%2FTechnical%20Data%20Sheets%2FC-Polyesters&openfile=21715.

[64] C.P. Ernst, K. Canbek, T. Euler, B. Willershausen, In vivo validation of the historical in vitro thermocycling temperature range for dental materials testing, Clin Oral Investig 8 (3) (2004) 130–138, https://doi.org/10.1007/s00784-004-0267-2.

[65] L. He, Y. Hao, L. Zhen, H. Liu, M. Shao, X. Xu, et al., Biomineralization of dentin, J. Struct. Biol. 207 (2) (2019) 115–122, https://doi.org/10.1016/j.jsb.2019.05.010.

[66] V. Vijayasankari, S. Asokan, P.R. GeethaPriya, Evaluation of remineralisation potential of experimental nano hydroxyapatite pastes using scanning electron microscope with energy dispersive X-ray analysis: an in-vitro trial, Eur. Arch. Paediatr. Dent. 20 (6) (2019) 529–536, https://doi.org/10.1007/s40368-018-00411-7.

[67] Technical Data Sheet of Extrudr PLA NX2 White, URL retrieved on 2024.05.16:https://s3-extrudr.mgh3.mynet.at/extrudr-media/datasheets/tds/tds-en/pla-nx2-TDS-en.pdf?response-content-disposition=attachment%3B+filename%3D%22pla-nx2-TDS-en.pdf%22.

[68] Technical Data Sheet of Prusament PETG, URL retrieved on 2024.05.20:https://storage.googleapis.com/prusa3d-content-prod-e8-wordpress-prusament-prod/2023/10/9f8d2165-tds_prusament-petg_n_en.pdf.

[69] P. Ball, Life's lessons in design, Nature 409 (6818) (2001) 413–416, https://doi.org/10.1038/35053198.

[70] A. Özen, D. Auhl, C. Völlmecke, J. Kiendl, B.E. Abali, Optimization of manufacturing parameters and tensile specimen geometry for fused deposition modeling (FDM) 3D-printed PETG, Materials 14 (10) (2021) 2556, https://doi.org/10.3390/ma14102556.

[71] A.H. Kadhum, S. Al-Zubaidi, S.S. Abdulkareem, Effect of the infill patterns on the mechanical and surface characteristics of 3D printing of PLA, PLA+ and PETG materials, ChemEngineering. 7 (3) (2023) 46, https://doi.org/10.3390/chemengineering7030046.

[72] A. Özen, B.E. Abali, C. Völlmecke, J. Gerstel, D. Auhl, Exploring the role of manufacturing parameters on microstructure and mechanical properties in fused deposition modeling (FDM) using PETG, Appl. Compos. Mater. 28 (6) (2021) 1799–1828, https://link.springer.com/article/10.1007/s10443-021-09940-9.

[73] M.T. Sepahi, H. Abusalma, V. Jovanovic, H. Eisazadeh, Mechanical properties of 3D-printed parts made of polyethylene terephthalate glycol, J. Mater. Eng. Perform. 30 (9) (2021) 6851–6861, https://doi.org/10.1007/s11665-021-06032-4.

[74] G. Holcomb, E.B. Caldona, X. Cheng, R.C. Advincula, On the optimized 3D printing and post-processing of PETG materials, MRS Communications 12 (3) (2022) 381–387, https://doi.org/10.1557/s43579-022-00188-3.

[75] D.A. Thomas, B.L. Averbach, The early stages of plastic deformation in copper, Acta Metall. 7 (2) (1959) 69–75, https://doi.org/10.1016/0001-6160(59)90110-5.

[76] C.Y. Ho, R.W. Powell, P.E. Liley, Thermal conductivity of the elements, J. Phys. Chem. Ref. Data 1 (2) (1972) 279–421, https://doi.org/10.1063/1.3253100.

[77] E.R. Fischer, B.T. Hansen, V. Nair, F.H. Hoyt, D.W. Dorward, Scanning electron microscopy, Curr Protoc Microbiol (2012), https://doi.org/10.1002/9780471729259.mc02b02s25 (Chapter 2):Unit 2B.

[78] G.E. Lloyd, Atomic number and crystallographic contrast images with the SEM: a review of backscattered electron techniques, Mineral. Mag. 51 (359) (1987) 3–19, https://doi.org/10.1180/minmag.1987.051.359.02.

[79] M.A. Saghiri, K. Asgar, M. Lotfi, K. Karamifar, A.M. Saghiri, P. Neelakantan, et al., Back-scattered and secondary electron images of scanning electron microscopy in dentistry: a new method for surface analysis, Acta Odontol. Scand. 70 (6) (2012) 603–609, https://doi.org/10.3109/00016357.2011.645057.

[80] P. Duncumb, P.K. Shields, The present state of quantitative X-ray microanalysis Part 1: physical basis, Br. J. Appl. Phys. 14 (10) (1963) 617, https://doi.org/10.1088/0508-3443/14/10/306.

[81] M. Scimeca, S. Bischetti, H.K. Lamsira, R. Bonfiglio, E. Bonanno, Energy Dispersive X-ray (EDX) microanalysis: a powerful tool in biomedical research and diagnosis, Eur. J. Histochem. 62 (1) (2018) 2841, https://doi.org/10.4081/ejh.2018.2841.

[82] J. Hwang, Y. Jeong, J.M. Park, K.H. Lee, J.W. Hong, J. Choi, Biomimetics: forecasting the future of science, engineering, and medicine, Int J Nanomedicine 10 (2015) 5701–5713.

[83] K. O'Hagan-Wong, J. Enax, F. Meyer, B. Ganss, The use of hydroxyapatite toothpaste to prevent dental caries, Odontology 110 (2) (2022) 223–230.

[84] J. Opydo-Szymaczek, T. Pawlaczyk-Kamieńska, M. Borysewicz-Lewicka, Fluoride intake and salivary fluoride retention after using high-fluoride toothpaste followed by post-brushing water rinsing and conventional (1400 & 1450 ppm) fluoride toothpastes used without rinsing, Int. J. Environ. Res. Publ. Health 19 (20) (2022) 13235, https://doi.org/10.3390/ijerph192013235.

[85] D. Moreno Nieto, M. Alonso-Garcia, M.A. Pardo-Vicente, L. Rodriguez-Parada, Product design by additive manufacturing for water environments: study of degradation and absorption behavior of PLA and PETG, Polymers 13 (7) (2021), https://doi.org/10.3390/polym13071036.

[86] I. Gendviliene, E. Simoliunas, M. Alksne, S. Dibart, E. Jasiuniene, V. Cicenas, et al., Effect of extracellular matrix and dental pulp stem cells on bone regeneration with 3D printed PLA/HA composite scaffolds, Eur. Cell. Mater. 41 (2021) 204–215, https://doi.org/10.22203/ecm.v041a15.

[87] H. Ren, X. Zhang, Y. Li, D. Zhang, F. Huang, Z. Zhang, Preparation of cross-sectional membrane samples for scanning electron microscopy characterizations using a new frozen section technique, Membranes 13 (7) (2023), https://doi.org/10.3390/membranes13070634.

[88] R.R. Ferlita, D. Phipps, J. Safarik, D.H. Yeh, Cryo-snap: a simple modified freeze-fracture method for SEM imaging of membrane cross-sections, Environ. Prog. 27 (2) (2008) 204–209, https://doi.org/10.1002/ep.10270.

[89] S. Park, K. Fu, Polymer-based filament feedstock for additive manufacturing, Compos. Sci. Technol. 213 (2021) 108876, https://doi.org/10.1016/j.compscitech.2021.108876.

[90] M. Puthumana, P. Santhana Gopala Krishnan, S.K. Nayak, Chemical modifications of PLA through copolymerization, Int. J. Polym. Anal. Char. 25 (8) (2020) 634–648, https://doi.org/10.1080/1023666X.2020.1830650.

[91] P.K. Penumakala, J. Santo, A. Thomas, A critical review on the fused deposition modeling of thermoplastic polymer composites, Compos. B Eng. 201 (2020) 108336, https://doi.org/10.1016/j.compositesb.2020.108336.